

2017-07

Semi-quantitative reconstruction of early to late Holocene spring and summer sea ice conditions in the northern Barents Sea

Berben, SMP

<http://hdl.handle.net/10026.1/9644>

10.1002/jqs.2953

Journal of Quaternary Science

Wiley

All content in PEARL is protected by copyright law. Author manuscripts are made available in accordance with publisher policies. Please cite only the published version using the details provided on the item record or document. In the absence of an open licence (e.g. Creative Commons), permissions for further reuse of content should be sought from the publisher or author.

1
2
3 1 **Semi-quantitative reconstruction of early to late Holocene spring and summer sea ice**
4 **conditions in the northern Barents Sea**
5
6
7 3

8 4 **Sarah M.P. Berben^{a,1}, Katrine Husum^b, Alba Navarro-Rodriguez^c, Simon T. Belt^c,**
9 **Steffen Aagaard-Sørensen^a**
10

11 ^a*Department of Geology, UiT – The Arctic University of Norway, N-9037 Tromsø, Norway*

12 ^b*Norwegian Polar Institute, Fram Centre, N-9296 Tromsø, Norway*

13 ^c*Biogeochemistry Research Centre, School of Geography, Earth and Environmental Sciences,*
14 *University of Plymouth, Drake Circus, Plymouth PL4 8AA, UK*
15
16
17
18

19 ¹Corresponding author.

20 E-mail address: sarah.berben@uib.no

21 Current address: Department of Earth Science, University of Bergen and the Bjerknes Centre
22 for Climate Research, N-5007 Bergen, Norway
23
24
25
26
27

28 **Abstract**

29 Semi-quantitative estimates of early to late Holocene spring sea ice concentration (SpSIC)
30 and occurrence of summer sea ice for the northern Barents Sea have been obtained by
31 analysing the biomarkers IP₂₅, brassicasterol and a tri-unsaturated highly branched isoprenoid
32 lipid in a Holocene marine sediment core. Sub-surface water mass variations were derived
33 from planktic foraminiferal assemblages and stable isotopes ($\delta^{18}\text{O}$, $\delta^{13}\text{C}$). The record indicates
34 paleoceanographic changes over three intervals. During Period I (ca. 9500–5900 cal a BP),
35 the study location experienced the lowest recorded SpSIC (ca. 25%) with short spring seasons
36 and long productive summers, resulting partly from increased Atlantic Water inflow that
37 caused a stronger ocean-atmosphere heat exchange. Throughout Period II (ca. 5900–2700 cal
38 a BP), the winter sea ice margin migrated southwards and an overall cooling trend resulted in
39 higher SpSIC (ca. 60%) and increased delivery of cold Arctic Water. During Period III (ca.
40 2700 cal a BP–present), SpSIC increased further (ca. 75%) and some sea ice remained during
41 summer months. A sub-surface warming likely indicates a decoupling of heat exchange
42 between the ocean and the atmosphere. Longer springs and shorter summers were
43 accompanied by the most southerly location of the winter sea ice margin.
44
45
46
47
48
49
50
51
52
53
54
55

56 **Keywords**

57 Sea ice, biomarker, proxy data, Holocene, Arctic
58
59
60

1
2
3 354
5 36 **Introduction**

6
7 37 The Barents Sea is a relatively small and shallow sea, yet it plays a crucial role in the Arctic
8
9 38 climate system, in part, because of significant heat exchange between the ocean and the
10
11 39 atmosphere (Serreze *et al.*, 2007). Oceanic heat is brought into the Barents Sea via the inflow
12
13 40 of warm Atlantic water and, due to shallow depths, heat loss to the atmosphere is very
14
15 41 efficient. Further, it has been suggested that ocean advection strongly influences sea ice
16
17 42 conditions in the Barents Sea, so the region is central to understanding ocean-sea ice-
18
19 43 atmosphere interactions (Vinje, 2001).

20
21 44 Recently, many Arctic regions have experienced an abrupt decline in sea ice conditions, with
22
23 45 the northern Barents Sea and the Chukchi Sea identified as the most affected areas during the
24
25 46 last three to four decades (Screen and Simmonds, 2010; Stroeve *et al.*, 2007, 2012). Present
26
27 47 day sea ice variations within the Barents Sea have been attributed to different processes (e.g.
28
29 48 atmospheric circulation variability, local wind patterns, ice import from the Arctic interior to
30
31 49 the Barents Sea), although the role of oceanic heat advection is often emphasized as one of the
32
33 50 most important factors (e.g. Årthun *et al.*, 2012; Ivanov *et al.*, 2012; Smedsrud *et al.*, 2013).
34
35 51 For example, Årthun *et al.* (2012) argued that recent increases in Atlantic Water inflow to the
36
37 52 Barents Sea has contributed to a further decline in sea ice conditions in the Barents Sea.
38
39 53 Similarly, the northerly inflow of Pacific Water has been suggested as a contributing factor to
40
41 54 reduced sea ice conditions in the Chukchi Sea in recent times (e.g. Shimada *et al.*, 2006;
42
43 55 Woodgate *et al.*, 2010) and during the Holocene (Stein *et al.*, 2016a).

44
45 56 Since the impacts of Arctic amplification and the associated sea ice decline (Serreze and
46
47 57 Francis, 2006; Screen and Simmonds, 2010) reach far beyond the Arctic region (Yang and
48
49 58 Christensen, 2012), it is clearly necessary to better understand the interaction between sea ice
50
51 59 production and water mass conditions, together with any natural variability that occurs
52
53 60 between them over longer time frames. Instrumental and observational records of past climate
54
55 61 variations in the Barents Sea reach back only ca. 100–150 years (Divine and Dick, 2006;
56
57 62 Smedsrud *et al.*, 2013), so longer-term records of sea ice and water mass conditions need to
58
59 63 be derived from proxy climate indicators archived in marine sediment cores. Such records
60
61 64 from the northern Barents Sea (e.g. Duplessy *et al.*, 2001; Lubinski *et al.*, 2001;
62
63 65 Risebrobakken *et al.*, 2011; Klitgaard Kristensen *et al.*, 2013), the western Barents Sea
64
65 66 (Berben *et al.*, 2014) and the Svalbard margin (e.g. Slubowska *et al.*, 2005; Rasmussen *et al.*,

1
2
3 67 2007; Spielhagen *et al.*, 2011; Müller *et al.*, 2012; Werner *et al.*, 2013) have demonstrated
4 68 various fluctuations of both the influence of Atlantic Water inflow to the Barents Sea and sea
5 69 ice conditions throughout the Holocene. The observed Holocene changes in the region have
6 70 mainly been attributed to insolation changes and further factors such as land-cover feedbacks
7 71 and coupled atmospheric-oceanic dynamics, in particular the northward penetration of
8 72 relatively warm Atlantic Water (Berger, 1978; Koç *et al.*, 1993; Kaufman *et al.*, 2004).
9 73 Additionally, insolation forcing has also been attributed to the long-term sea ice variability
10 74 (Müller *et al.*, 2012; Cabedo-Sanz *et al.*, 2016b). However, few of these reconstructions have
11 75 employed a specific proxy for sea ice or have provided detailed descriptions of sea ice
12 76 conditions, including semi-quantitative estimates of spring sea ice concentration (SpSIC) or
13 77 summer sea ice occurrence.

14
15
16
17
18
19
20
21
22 78 In this study, the biomarkers IP₂₅, brassicasterol and a tri-unsaturated highly branched
23 79 isoprenoid (HBI) lipid (HBI III) have been analyzed in a marine sediment core from the Olga
24 80 Basin in order to reconstruct a detailed record of sea ice conditions for the early to late
25 81 Holocene in the northern Barents Sea (Fig. 1). The biomarker concentration data were
26 82 presented previously by Belt *et al.* (2015), but were not discussed in detail. In the current
27 83 study, therefore, we provide a more in-depth discussion of the individual and combined (i.e.
28 84 PIP₂₅) biomarker data, including, for the first time, semi-quantitative estimates of SpSIC
29 85 based on the recent calibration study by Smik *et al.* (2016). In addition, and similar to Werner
30 86 *et al.* (2013, 2014), planktic foraminiferal fauna assemblages and stable carbon and oxygen
31 87 isotopes ($\delta^{18}\text{O}$, $\delta^{13}\text{C}$) have also been measured to obtain a combined multiproxy record of sea
32 88 ice conditions and sub-surface water masses, thus demonstrating the interaction of sea ice and
33 89 inflow of Atlantic Water. The study site is located between the Atlantic Water characterized
34 90 southern Barents Sea and the central Arctic Ocean and is, therefore, influenced by Atlantic
35 91 derived water masses (Abrahamsen *et al.*, 2006) but also experiences seasonal sea ice
36 92 conditions (Fig. 1). As such, it represents a key location for reconstructing Holocene changes
37 93 in sea ice conditions and Atlantic Water inflow. Using our Holocene proxy data, we also
38 94 propose different oceanographic scenarios that emphasize the changing interactions between
39 95 sea ice conditions and near-surface waters and these are discussed further by comparing the
40 96 proxy data with outcomes from previous studies from the region.

41
42
43
44
45
46
47
48
49
50
51
52
53
54
55
56
57
58
59
60

97
98 *Sea ice biomarker background information*

1
2
3 99 Following the initial discovery of the Arctic sea ice proxy IP₂₅ (Belt *et al.*, 2007), analysis of
4
5 100 this biomarker has subsequently led to sea ice reconstructions for various sub-Arctic and
6
7 101 Arctic regions: the central Arctic Ocean (Xiao *et al.*, 2015a, 2015b), the Labrador Sea
8
9 102 (Weckström *et al.*, 2013), the Canadian Arctic (Vare *et al.*, 2009), the Bering Sea/North
10
11 103 Pacific (Méheust *et al.*, 2013, 2015), the Chukchi Sea (Polyak *et al.*, 2016; Stein *et al.*,
12
13 104 2016a), the East Siberian Sea (Stein *et al.*, 2016a), the Laptev Sea (Fahl and Stein 2012; Xiao
14
15 105 *et al.*, 2013), the Barents Sea (Vare *et al.*, 2010; Berben *et al.*, 2014), the Fram Strait (Müller
16
17 106 *et al.*, 2009, 2012; Cabedo-Sanz *et al.*, 2013, 2016a; Knies *et al.*, 2014; Müller and Stein,
18
19 107 2014) and the Greenland/Norwegian Seas (Massé *et al.*, 2008; Cabedo-Sanz *et al.*, 2016b).
20
21 108 Furthermore, IP₂₅ appears stable within Arctic sediments to permit sea ice reconstructions
22
23 109 over even longer timescales (e.g. going back into the Pliocene (Knies *et al.*, 2014) and the
24
25 110 Miocene (Stein *et al.*, 2016b). IP₂₅ is biosynthesized by certain Arctic sea ice diatoms and is
26
27 111 thus usually found in areas with seasonal sea ice conditions (e.g. Belt *et al.*, 2007; Brown *et*
28
29 112 *al.*, 2011, 2014; Belt and Müller, 2013). In order to provide complementary information
30
31 113 regarding open water conditions, Müller *et al.* (2009) proposed the additional measurement of
32
33 114 phytoplankton biomarkers, such as brassicasterol. In addition, by combining IP₂₅ and
34
35 115 phytoplankton biomarker concentrations, in the form of the so-called PIP₂₅ index, a method of
36
37 116 elucidating semi-quantitative estimates of sea ice conditions has been proposed (Müller *et al.*,
38
39 117 2011). However, application of the PIP₂₅ method is not always straightforward because some
40
41 118 phytoplankton markers such as brassicasterol may also have non-pelagic sources and their
42
43 119 generally higher concentration compared to IP₂₅ requires the use of a balance factor in the
44
45 120 calculation of PIP₂₅, which can be problematic (for a detailed discussion, see Belt and Müller,
46
47 121 2013; Navarro-Rodriguez *et al.*, 2013; Belt *et al.*, 2015; Xiao *et al.*, 2015a; Smik *et al.*, 2016).
48
49 122 A recent study by Belt *et al.* (2015), however, demonstrated that a further phytoplankton-
50
51 123 derived HBI biomarker, more specifically HBI III, was relatively abundant for locations
52
53 124 within the marginal ice zone or close to the winter ice margin in the Barents Sea, thus
54
55 125 representing an alternative indicator of open water conditions. In addition, since HBI III has a
56
57 126 more constrained source (diatoms) and has sedimentary concentrations much closer to those
58
59 127 of IP₂₅, some of the problems associated with using some other phytoplankton biomarkers can
60
128 potentially be avoided. In a subsequent study, Smik *et al.* (2016) also demonstrated that PIP₂₅
129 values based on IP₂₅ and HBI III could provide realistic estimates of SpSIC for the Barents
130 Sea, while a threshold value of 0.8 was suggested as providing evidence for the presence of
131 summer sea ice (>5% summer sea ice concentration (SuSIC)).

1
2
3 132
4
56 133 **Study area and oceanographic setting**

7
8 134 The Barents Sea is an epicontinental shelf located between the Norwegian-Russian coast,
9 135 Novaya Zemlya and the Svalbard and Franz Josef Land archipelagos (Fig. 1). The northern
10 136 boundary of the Barents Sea is defined by the Nansen Basin continental slope (Jakobsson *et*
11 137 *al.*, 2004). The Barents Sea is characterized by several water masses and represents a major
12 138 passage for Atlantic Water entering the Arctic Ocean (Carmack *et al.*, 2006; Rudels *et al.*,
13 139 2014).

14
15
16
17
18
19 140 The Norwegian Atlantic Current transports relatively warm and saline Atlantic Water towards
20 141 the high latitude North Atlantic Ocean (Hopkins, 1991) (Fig. 1a). Before entering the Barents
21 142 Sea, the Norwegian Atlantic Current splits into two different branches, the West Spitsbergen
22 143 Current and the North Cape Current, respectively (Fig. 1a). Both of these currents transport
23 144 the warm saline Atlantic Water into the Arctic Ocean (Rudels *et al.*, 2014). Within the
24 145 Barents Sea, Atlantic Water is entered from both the north and the southwest. The West
25 146 Spitsbergen Current flows northwards along the western Barents Sea slope and splits into
26 147 three branches in the Fram Strait; the Return Atlantic Current, the Yermak Branch and the
27 148 Svalbard Branch (Fig. 1a) (e.g. Manley, 1995). The latter enters the Arctic Ocean north of
28 149 Svalbard as a sub-surface current flowing eastward and beyond the Franz Victoria and St.
29 150 Anna Troughs (Abrahamsen *et al.*, 2006; Rudels *et al.*, 2014). A sub-surface inflow of
30 151 Atlantic Water derived from the Svalbard Branch enters the Barents Sea via the Northern
31 152 Barents Sea Opening (Fig. 1a). Subsequently, Atlantic Water is advected south-westwards
32 153 into the northern Barents Sea and has been observed year-round in the Olga Basin
33 154 (Abrahamsen *et al.*, 2006) where the studied sediment core is located. Although the major
34 155 sub-surface water mass in the Olga Basin is Atlantic Water derived from the Svalbard Branch
35 156 (Gammelsrød *et al.*, 2009; Klitgaard Kristensen *et al.*, 2013), the area is furthermore
36 157 influenced by Atlantic Water that enters as a submerged flow from the south (e.g. Novitskiy,
37 158 1961; Loeng, 1991; Pfirman *et al.*, 1994; Aksenov *et al.*, 2010). The latter is brought to the
38 159 area by the North Cape Current flowing northwards via the Barents Sea Opening into the
39 160 southern Barents Sea, parallel to the coastal current system (Loeng, 1991; Loeng *et al.*, 1993;
40 161 Midttun, 1985; Rudels, 1987) (Fig. 1a). After mixing and heat loss, Atlantic Water exits the
41 162 Barents Sea via the Barents Sea Exit and reaches the Arctic Ocean via the St. Anna Trough
42 163 (e.g. Schauer *et al.*, 2002; Rudels *et al.*, 2014) (Fig. 1a).

1
2
3 164 In addition to relatively warm Atlantic Water, the Barents Sea is also influenced by Polar
4
5 165 Water that is brought from the Arctic Ocean into the Barents Sea through the Franz Victoria
6
7 166 and St. Anna Troughs, via the East Spitsbergen Current and the Bear Island Current,
8
9 167 respectively (Hopkins, 1991) (Fig. 1a). Arctic Water is formed when relatively warm Atlantic
10
11 168 Water converges and merges with cold, less saline and ice loaded Polar Water (Hopkins,
12
13 169 1991). Hence, surface water in the north-eastern Barents Sea is, in contrast to the Atlantic
14
15 170 Water dominated south-western Barents Sea, dominated by Arctic Water characterized by
16
17 171 reduced temperature and salinity, as well as seasonal sea ice conditions (Hopkins, 1991). A
18
19 172 CTD profile taken at the core location illustrates the presence of Arctic Water at the surface,
20
21 173 with Atlantic Water below ca. 150 m (Fig. 1c; Table S1).

22
23 174 The oceanic fronts dividing these different water masses are one of the main oceanographic
24
25 175 features of the near-surface waters of the Barents Sea (Pfirman *et al.*, 1994). Defined as a
26
27 176 sharp climatic gradient in terms of temperature, salinity and sea ice conditions, the Polar and
28
29 177 Arctic fronts are the respective boundaries between Polar/Arctic and Arctic/Atlantic waters.
30
31 178 The positions of the Polar and Arctic fronts are closely related to the overall sea ice conditions
32
33 179 and, in particular, align with the average summer and winter sea ice margins, respectively
34
35 180 (Vinje, 1977). Although sea ice advection from the Arctic Ocean does occur, sea ice within
36
37 181 the Barents Sea is mainly formed locally during autumn and winter (Loeng, 1991). The
38
39 182 southward extent of the oceanic fronts, and hence the sea ice conditions in particular, are
40
41 183 regulated by the inflow of Atlantic Water into the western Barents Sea, which controls the
42
43 184 mainly ice-free Atlantic domain in the south-western Barents Sea (Årthun *et al.*, 2012). In
44
45 185 contrast, the north-eastern Barents Sea experiences large changes in seasonal sea ice
46
47 186 conditions (Vinje, 2001; Sorteberg and Kvingedal, 2006) with maximum sea ice conditions
48
49 187 during March/April and minimum occurring throughout August/September (Fig. 1b). Annual
50
51 188 sea ice variability during recent decades might be explained by factors such as cyclone
52
53 189 activity, which cause fluctuations in sea ice transport, to and from the Arctic Ocean into the
54
55 190 north-eastern Barents Sea (Kwok *et al.*, 2005; Sorteberg and Kvingedal, 2006; Ellingsen *et*
56
57 191 *al.*, 2009; Kwok, 2009).

58
59 192 The interplay between water masses and other influences that impact sea ice formation in the
60
193 Barents Sea determine the position of the marginal ice zone, an area characterized by high
194
195 surface productivity during the summer season (e.g. Smith and Sakshaug, 1990). Within the
196
197 Barents Sea, enhanced primary production results from a peak algal bloom along the ice
198
199 margin during spring as sea ice retreats (Sakshaug *et al.*, 1992). In addition, the advection of

1
2
3 197 Atlantic Water contributes to longer productive seasons, compared to other Arctic areas
4 198 (Wassmann, 2011). Consequently, the Barents Sea is one of the most productive areas of the
5
6 199 Arctic Seas (Wassmann *et al.*, 2006; Wassmann, 2011).
7
8
9 200

11 201 **Material and methods**

12
13
14 202 A 245 cm long marine sediment core NP05-11-70GC was retrieved in 2005 by the RV *Lance*
15 203 south of Kong Karls Land (Olga Basin) within the northern Barents Sea (78.40° N, 32.42° E;
16 204 293 m water depth) using a gravity coring device (Fig. 1). The upper section of the core (0–
17 205 124 cm; 1-cm intervals) was investigated in the current study and was characterized by
18 206 homogeneous sediments rich in silty clay deposited in a marine environment.
19
20
21
22
23 207

25 208 *Chronology*

26
27
28 209 A depth-age model for NP05-11-70GC was developed using linear interpolation between
29 210 three calibrated AMS ¹⁴C dates obtained from mixed benthic foraminifera as described by
30 211 Berben (2014) and Belt *et al.* (2015) (Fig. 2; Table 1; Table S2). In order to try and improve
31 212 the age control, attempts to obtain more ¹⁴C dates were made by collecting all benthic
32 213 foraminifera at each core level selected for microfossil analyses (i.e. every cm).
33 214 Unfortunately, additional ¹⁴C measurements were prevented due to the very low numbers of
34 215 foraminifera (and thus insufficient amounts of CaCO₃ (Fig. 4)). Nonetheless, the lithological
35 216 description of a marine sediment core from a very nearby location in the northern Barents Sea
36 217 also indicate a well-defined homogeneous unit corresponding to Holocene sediments
37 218 (Klitgaard Kristensen *et al.*, 2013). Thus, based on lithological similarities, together with
38 219 some younger AMS ¹⁴C dates (<2000 cal a BP) in a nearby core, the NP05-11-70GC core top
39 220 is assumed to represent modern age. The AMS ¹⁴C dates were calibrated using Calib 6.1.1
40 221 (Stuiver and Reimer, 1993) and the Marine09 calibration curve (Reimer *et al.*, 2009). A local
41 222 reservoir age (ΔR) of 105±24 suggested for the Svalbard area by Mangerud *et al.* (2006) was
42 223 used in the calibration (Table 1).
43
44
45
46
47
48
49
50
51
52
53

54 224 55 56 225 *Biomarker analysis*

1
2
3 226 To reconstruct past sea ice conditions, the seasonal sea ice biomarker IP₂₅ and the open water
4
5 227 phytoplankton biomarkers (brassicasterol and HBI III) were analysed in 49 sub-samples (ca. 1
6
7 228 g taken from the same bulk sediment samples used for foraminiferal analysis). Prior to
8
9 229 analysis, sub-samples were freeze-dried and stored at -20 °C. The general methodology for
10
11 230 biomarker extraction, purification and analysis was as previously described by Belt *et al.*
12
13 231 (2012) and Brown and Belt (2012). Analytical reproducibility was monitored using a
14
15 232 sediment with known biomarker concentrations for every 10–12 extracted sediment samples
16
17 233 (analytical error <6%, n=5). Lipid quantification was conducted using the integrated peak
18
19 234 areas of each biomarker and the internal standard, an instrumental response factor, and the
20
21 235 masses of the extracted sediment and internal standard (Belt *et al.*, 2012). Biomarker
22
23 236 concentrations, normalized to dry weight sediment mass (µg/g sed.) as presented previously
24
25 237 (Belt *et al.*, 2015), were further normalized to total organic carbon (µg/g TOC) in order to
26
27 238 compensate possible regional differences in production and degradation in sediments (Belt
28
29 239 and Müller, 2013). The weight percentages (wt. %) of TOC (n=43) were determined using a
30
31 240 Carlo Erba EA 1110 elemental analyzer at Plymouth University. In order to remove any
32
33 241 inorganic carbonate, ca. 100 mg of freeze-dried sediment was digested in HCl (1mL; 18h).

34
35 242 To investigate past sea ice conditions more quantitatively, IP₂₅ and phytoplankton biomarkers
36
37 243 were used to calculate the so-called P_BIP₂₅ and P_{III}IP₂₅ indices (i.e. PIP₂₅ based on
38
39 244 brassicasterol and HBI III, respectively) (Müller *et al.*, 2011; Belt *et al.*, 2015). Calculation of
40
41 245 the P_BIP₂₅ index was achieved using Eq. 1, which includes a concentration balance factor (*c*;
42
43 246 Eq. 2) to compensate for the significant concentration difference between IP₂₅ and
44
45 247 brassicasterol (Müller *et al.*, 2011).

$$46 \quad 248 \quad P_{BIP_{25}} = IP_{25} / (IP_{25} + (\text{brassicasterol} * c)) \quad [\text{Eq. 1}]$$

$$47 \quad 249 \quad c = \text{mean IP}_{25} / \text{mean brassicasterol} \quad [\text{Eq. 2}]$$

48
49 250 Calculation of P_{III}IP₂₅ indices was achieved by replacing brassicasterol concentrations (Eq. 1)
50
51 251 with those of HBI III. The balance factor, *c*, was calculated according to the relative mean
52
53 252 concentrations of IP₂₅ and HBI III (i.e. as per brassicasterol; Eq. 2) and we also used a value
54
55 253 of 0.63, derived from a regional calibration of surface sediments from the Barents Sea (Belt *et*
56
57 254 *al.*, 2015; Smik *et al.*, 2016). In practice, P_{III}IP₂₅ values using a *c* term based on Eq. 2 (0.84)
58
59 255 were very similar to those using the value of *c* derived from the surface sediment calibration
60
256 (0.63; Smik *et al.*, 2016). For simplicity, we present data using the surface sediment

1
2
3 257 calibration only. Semi-quantitative estimates of SpSIC were also made using the P_{III}IP₂₅ data
4 258 and the calibration of Smik *et al.* (2016) (Eq. 3) (for more background information, see
5 259 Introduction).

6
7
8
9 260
$$\text{SpSIC (\%)} = (\text{P}_{\text{III}}\text{IP}_{25} - 0.0692) / 0.0107 \quad [\text{Eq. 3}]$$

10
11 261

12
13
14 262 *Planktic foraminifera*

15
16
17 263 The sediment core was opened, and the sediments were sampled and frozen within 48 hours.
18 264 Sediment samples were freeze-dried, wet-sieved through three different size fractions (1000,
19 265 100 and 63 μm), and dried at 40 °C. Planktic foraminiferal assemblages were determined for
20 266 123 samples using the 100–1000 μm size fraction following Knudsen (1998). Following
21 267 Forcino (2012), the relative abundances (%) of each species were calculated for samples
22 268 containing more than 25 specimens (82 samples). Identification of *Neogloboquadrina*
23 269 *pachyderma* and *Neogloboquadrina incompta* species was achieved following Cifelli (1961)
24 270 and Darling *et al.* (2006), and planktic foraminiferal concentrations (#/g sed.) were calculated.

25
26
27
28
29
30
31 271 As the planktic foraminiferal assemblages might be affected by carbonate dissolution, it is
32 272 important to assess the impact of preservation changes on the planktic foraminiferal data (e.g.
33 273 Zamelczyk *et al.*, 2013). Here, the preservation conditions were investigated by analysing
34 274 preservation indicators such as the mean shell weight of *N. pachyderma* and the percentage of
35 275 fragmentation of planktic foraminiferal tests. A loss in the mean shell weight can be used to
36 276 identify dissolution in the water column and sediment surface (Broecker and Clark, 2001;
37 277 Barker and Elderfield, 2002; Barker *et al.*, 2004). Hence, 25 well preserved (visually) and
38 278 square shaped *N. pachyderma* specimens were picked from each sample from a narrow size
39 279 range (150–250 μm) in order to reduce problems of ontogeny and size difference induced
40 280 variability (Barker *et al.*, 2004). It was possible to obtain a mean shell weight (μg) of the 25
41 281 picked specimens per sample of *N. pachyderma* using a Mettler Toledo microbalance (0.1 μg
42 282 sensitivity; 110 samples). Further, the degree of fragmentation indicates the dissolution
43 283 induced weakening of the tests as well as dissolution processes within the sediment (Conan *et*
44 284 *al.*, 2002). The fragmentation (%) of planktic foraminiferal tests was calculated for the 82
45 285 samples that contained a total number of >25 specimens within the 100–1000 μm size
46 286 fraction. The fragmentation was calculated using the equation proposed by Pfuhl and
47 287 Shackleton (2004) (Eq. 4).

1
2
3 288 Fragmentation = ((#fragments/g) / ((#fragments/g/3) + (#tests/g))) * 10 [Eq. 4]
4
5
6

7
8
9 289

10 290 *Stable carbon and oxygen isotope analysis*

11 291 The stable carbon and oxygen isotopic compositions of planktic foraminiferal shells ($\delta^{18}\text{O}$,
12 292 $\delta^{13}\text{C}$) are widely used to reflect the ambient sea water mass properties in which they have
13 293 been calcified. In particular, $\delta^{18}\text{O}$ is a proxy for temperature and salinity, whereas $\delta^{13}\text{C}$
14 294 variations reflect primary production and stratification changes (e.g. Spielhagen and
15 295 Erlenkeuser, 1994; Katz *et al.*, 2010). The $\delta^{18}\text{O}$ and $\delta^{13}\text{C}$ analyses were performed on the
16 296 foraminiferal tests of *N. pachyderma*. All specimens were selected from a narrow size range
17 297 (150–250 μm) in order to minimize size dependent effects on isotopic composition (Aksu and
18 298 Vilks, 1988; Keigwin and Boyle, 1989; Oppo and Fairbanks, 1989; Donner and Wefer, 1994;
19 299 Bauch *et al.*, 2000). Sufficient amount of specimens were obtained from 105 samples.
20 300 Samples were analysed using a Finnigan MAT 253 mass spectrometer coupled to an
21 301 automated Kiel IV Carbonate Preparation Device at the Geological Mass Spectrometer
22 302 (GMS) Laboratory at the University of Bergen. These measurements were conducted with a
23 303 reproducibility of ± 0.06 ‰ ($\delta^{18}\text{O}$) and ± 0.03 ‰ ($\delta^{13}\text{C}$). Data are reported on the ‰ versus
24 304 VPDB scale calibrated with NBS-19. Corrections for the ice volume effect were applied on
25 305 the measured $\delta^{18}\text{O}$ values according to Fairbanks (1989). No vital effect corrections were
26 306 applied for the isotope measurements in this study as published estimates of species-specific
27 307 vital effects are often inconsistent (e.g. Kohfeld *et al.*, 1996; Bauch *et al.*, 1997; Stangeew,
28 308 2001; Simstich *et al.*, 2003), possibly due to seasonal changes of the apparent vital effect
29 309 (Jonkers *et al.*, 2010).

30
31
32
33
34
35
36
37
38
39
40
41
42
43 310

44 311 **Results**

45
46
47 312 The resulting depth-age model ranges between the present and ca. 9400 cal a BP (Fig. 2). The
48 313 depth-age model presented here has its limitations (for a detailed discussion, see Chronology)
49 314 and hence, for this reason, assigned ages should be taken with caution. Therefore, all data
50 315 plots presenting the results of this study also include a depth scale, although the results are
51 316 described with respect to age to enable us to place them into a wider context, both spatially
52 317 and temporally, when comparing them with previously published results. Despite the
53
54
55
56
57
58
59
60

1
2
3 318 limitations of the age control, which prevents the determination of centennial-scale changes,
4 319 we believe it is nonetheless feasible to describe the general early to late Holocene changes
5 320 with some confidence.
6
7
8 321

9
10 322 *Biomarker data*
11

12
13 323 The initial decrease in IP₂₅ concentrations (2 data points) followed by low values, coincides
14 324 with increased concentrations of both brassicasterol and HBI III ca. 9500–8500 cal a BP (Fig.
15 325 3a-c; Table S3). Hereafter, IP₂₅ concentrations show slightly higher values, whereas
16 326 brassicasterol and HBI III show decreased concentrations towards ca. 5900 cal a BP (Fig. 3a-
17 327 c). During this entire time interval (i.e. ca. 9500–5900 cal a BP), a decreasing trend in TOC is
18 328 also observed, although values remain relatively high (Fig. 3d; Table S3). From ca. 5900–
19 329 2700 cal a BP, the concentration of IP₂₅ increases further, while brassicasterol and HBI III
20 330 both decrease although TOC values remain relatively stable (Fig. 3a-d). The last ca. 2700 cal
21 331 a BP are characterized by the highest concentrations of IP₂₅ and relatively low (but stable)
22 332 concentrations of brassicasterol and HBI III (Fig. 3a-c). Although the TOC values fluctuate
23 333 somewhat throughout this period, the absolute values are the lowest within the entire record
24 334 (Fig. 3d).

25
26
27
28
29
30
31
32
33
34 335 Both P_BIP₂₅ and P_{III}IP₂₅ indices, as well as the estimated SpSIC (which is linearly related to
35 336 P_{III}IP₂₅; Smik *et al.*, 2016), follow the same trends throughout the entire record (Fig. 3e-g;
36 337 Table S3). After the initial lowest values at ca. 9000 cal a BP, each of P_BIP₂₅, P_{III}IP₂₅ and
37 338 SpSIC show increasing (although still relatively low) values towards ca. 5900 cal a BP (Fig.
38 339 3e-g). The mean SpSIC estimate ca. 9500–5900 cal a BP is ca. 25% (Fig. 3g). From ca. 5900–
39 340 2700 cal a BP, the P_BIP₂₅, P_{III}IP₂₅ and SpSIC records continue their increasing trend, albeit
40 341 more gradually. The estimated SpSIC shows a mean value of ca. 60% throughout this time
41 342 interval (Fig. 3g) with highest values towards ca. 2700 cal a BP. The P_BIP₂₅ reaches its
42 343 highest value at the core top, whereas the P_{III}IP₂₅ records a maximum value at ca. 1600 cal a
43 344 BP after which it remains high until the present (Fig. 3e-f). Estimates of SpSIC show a mean
44 345 value of ca. 75% (Fig. 3g). According to the threshold limit (P_{III}IP₂₅>0.8) suggested by Smik
45 346 *et al.* (2016), the occurrence of summer sea ice (SuSIC>5%) is estimated to have begun ca.
46 347 2700 cal a BP and remained a consistent feature thereafter, until the present (Fig. 3f).

47
48
49
50
51
52
53
54
55
56 348
57
58
59
60

1
2
3 349 *Planktic foraminiferal preservation*
4

5
6 350 From ca. 9500–7300 cal a BP, the absolute abundances of planktic foraminifera remain
7
8 351 relatively low where after, they increase towards 5900 cal a BP (Fig. 4a; Table S4). From ca.
9
10 352 5900–2700 cal a BP, the planktic foraminiferal concentration has a broader range (Fig. 4a),
11
12 353 while in the last ca. 2700 cal a BP, three episodes of increased planktic foraminiferal
13
14 354 concentration values are observed ca. 2400–2000 cal a BP, ca. 1600–700 cal a BP, and ca.
15
16 355 400 cal a BP–present (Fig. 4a).

17
18 356 From ca. 9500–5900 cal a BP, the extent of fragmentation shows a mean value of 32%,
19
20 357 whereas the mean shell weight is highly variable until ca. 7300 cal a BP, followed by more
21
22 358 stable values (ca. 7.5 µg) towards ca. 5900 cal a BP (Fig. 4b-c; Table S4). The mean shell
23
24 359 weight remains relatively stable (ca. 7 µg) ca. 5900–2700 cal a BP, while the fragmentation
25
26 360 record exhibits an overall decrease (Fig. 4b-c). During the last ca. 2700 cal a BP, the degree of
27
28 361 fragmentation shows a small overall increase although there is mainly an increase in the
29
30 362 amplitude (i.e. minima and maxima between ca. 9–83%) (Fig. 4b). At the same time, the
31
32 363 mean shell weight shows a general decrease (Fig. 4c).

33
34
35 364

36
37 365 *Planktic foraminiferal fauna*
38

39
40 366 The planktic foraminiferal record is characterized by the presence of polar (*N. pachyderma*)
41
42 367 and sub-polar (*N. incompta*, *Turborotalita quinqueloba*, *Globigerinita glutinata*, *Globigerina*
43
44 368 *bulloides* and *Globigerinita. uvula*) species with *N. pachyderma* generally dominating the
45
46 369 assemblages (Fig. 4d-i; Table S4). From ca. 9500–7300 cal a BP, the fauna is dominated by
47
48 370 *N. pachyderma* (ca. 95%) followed by a period (ca. 7300–5900 cal a BP) with increased
49
50 371 relative abundances of *T. quinqueloba*, *N. incompta* and *G. glutinata* up to ca. 24, 27 and 4%,
51
52 372 respectively (Fig. 4d-g). After ca. 5900 cal a BP, the relative abundances of *T. quinqueloba*
53
54 373 and *N. incompta* decrease and remain relatively stable (ca. 3–4%) towards ca. 2700 cal a BP,
55
56 374 while *N. pachyderma* clearly dominates the planktic foraminiferal fauna (Fig. 4d-f).
57
58 375 Throughout the last ca. 2700 cal a BP, a reduction in *N. pachyderma* (towards ca. 65%) is
59
60 376 accompanied by increasing relative abundances of *G. glutinata* (ca. 5%) and *G. bulloides* (ca.
377
378 8%), whereas *T. quinqueloba* and *N. incompta* reach their highest values between ca. 2400–
2000 cal a BP, ca. 1600–700 cal a BP and ca. 400 cal a BP–present (Fig. 4d-h). The period

1
2
3 379 from ca. 400 cal a BP–present is characterized by a clear increase of *G. glutinata* (ca. 7%) and
4 380 *G. bulloides* (ca. 6%), in addition to a remarkable increase of *G. uvula* (ca. 7%) (Fig. 4g-i).

5
6
7 381

8
9
10 382 *Stable carbon and oxygen isotope data*

11
12 383 From ca. 9500–8800 cal a BP, the $\delta^{18}\text{O}$ (*N. pachyderma*) record has a mean value of 3.8 ‰
13 384 followed by a period (ca. 8800–7300 cal a BP) characterized by lighter values (Fig. 5a; Table
14 385 S5). A significant increase in $\delta^{18}\text{O}$ ca. 7600–7300 cal a BP is followed by heavier values that
15 386 fluctuate around ca. 3.7 ‰ until ca. 5900 cal a BP. The $\delta^{18}\text{O}$ record remains relatively stable
16 387 ca. 5900–2700 cal a BP with relatively heavy values (Fig. 5a). Throughout the last ca. 2700
17 388 cal a BP, the $\delta^{18}\text{O}$ record shows decreased values in the range 3.5–4.0 ‰ (Fig. 5a).

18
19
20
21
22
23 389 The $\delta^{13}\text{C}$ record shows a decrease from 0.4 to 0.0 ‰ ca. 9500–8500 cal a BP (Fig. 5b; Table
24 390 S5). This trend is reversed at ca. 8500 cal a BP, with heavier $\delta^{13}\text{C}$ values towards ca. 5900 cal
25 391 a BP followed by an increase towards 0.9 ‰ ca. 5900–2700 cal a BP (Fig. 5b). The last ca.
26 392 2700 cal a BP are then characterized by a decreasing trend with $\delta^{13}\text{C}$ values in the range 0.3–
27 393 0.8 ‰ (Fig. 5b).

28
29
30
31
32 394

33
34
35 395 **Discussion**

36
37 396 Throughout the early to late Holocene, the palaeoceanographic record in NP05-11-70GC
38 397 shows an overall increase in sea ice reflecting the decline in solar insolation (Fig. 6a-d).
39 398 Related IP25-based reconstructions have been reported for other Arctic and sub-Arctic
40 399 regions such as the Fram Strait, the Laptev Sea, the East Siberian Sea and the Chukchi Sea
41 400 (Stein *et al.*, 2016a), as well as for the Canadian Arctic (Vare *et al.*, 2009; Belt *et al.*, 2010)
42 401 and North Iceland (Cabedo-Sanz *et al.*, 2016b). However, for some other regions, including
43 402 the Alaskan margin (Polyak *et al.*, 2016) and the western Barents Sea (Berben *et al.*, 2014),
44 403 this long-term trend is not as evident. The record presented here for the northern Barents Sea
45 404 is described in terms of individual time intervals reflecting the main stages of sea ice
46 405 conditions and Atlantic Water inflow. The intervals are: Period I (ca. 9500–5900 cal a BP),
47 406 Period II (ca. 5900–2700 cal a BP) and Period III (ca. 2700 cal a BP–present), although the
48 407 interpretation of the timing of the exact boundaries between these intervals should be
49 408 considered with caution due to the limitations of the age-depth model (see Chronology).

1
2
3 409 Climate and oceanographic variations during these periods are discussed and set into further
4 410 context by comparison with previously published records from the region.

5
6
7 411 Our interpretation of the sea ice conditions involves the identification of previously
8 412 unavailable semi-quantitative estimates of SpSIC and summer sea ice occurrence using a
9 413 recently calibrated biomarker approach, which has also permitted the proposal of different sea
10 414 ice scenarios. To obtain realistic representations for such sea ice conditions, known scenarios
11 415 derived from modern and historical observations of the Barents Sea (NSIDC) have been
12 416 considered (Fig. 1b). For example, the modern sea ice conditions have been derived from
13 417 maximum (March) and seasonal variability (April/August) in sea ice using satellite data
14 418 obtained between 1981 and 2010 (NSIDC) (Fig. 7c). In terms of temporal changes, historical
15 419 data from the Barents Sea show variations in the mean sea ice margin position in April for
16 420 four sub-periods between 1870 and 2002 (Divine and Dick, 2006). A north-easterly retreat of
17 421 the sea ice margin since the second half of the 19th century occurred after a significant cooling
18 422 in the second half of the 18th century (Divine and Dick, 2006) (Fig. 1b). This historical data
19 423 from the Barents Sea illustrates that the decadal migration pattern of the sea ice margins
20 424 associated with climatic conditions can reflect observed sea ice changes on an annual and/or
21 425 seasonal time scale. Therefore, this key dataset provides precedent for the proposed sea ice
22 426 scenarios (and changes to these) within the Barents Sea during the early to late Holocene.

23
24
25 427 With respect to the planktic foraminiferal preservation conditions, the proxy data is
26 428 interpreted as follows. Better calcium carbonate preservation has been associated with
27 429 increased production of organic matter in regions impacted by Atlantic Water (e.g. Hebbeln *et al.*
28 430 *al.* 1998; Henrich *et al.* 2002). In particular, for areas with enhanced Atlantic Water inflow
29 431 towards the Fram Strait, ocean currents appear to have a positive influence on the
30 432 preservation of organic matter in sediments (Birgel and Stein, 2004; Birgel *et al.*, 2004). The
31 433 wide range in both fragmentation and mean shell weight could therefore reflect variable
32 434 environmental control, preservation conditions or a combination of both. The high mean shell
33 435 weight ca. 7300–5900 cal a BP indicates better preservation conditions, possibly related to an
34 436 increased influence of Atlantic Water (Fig. 4c). In contrast, throughout the last ca. 2700 cal a
35 437 BP, the preservation indicators (i.e. low mean shell weight and highly fluctuating
36 438 fragmentation) show an overall change towards enhanced dissolution (Fig. 4b-c). This may be
37 439 caused by an increased influence of sea ice formation and brine rejection which may form
38 440 corrosive bottom water masses causing dissolution at the sea floor (e.g. Midttun 1985;
39 441 Steinsund and Hald 1994). Further, the low planktic foraminiferal concentrations may seem to

1
2
3 442 indicate poor preservation conditions, however studies of recent planktic foraminifera show
4 443 that low planktic foraminiferal concentrations can be found within environments
5 444 characterized by sea ice conditions (Carstens *et al.* 1997; Pados and Spielhagen 2014). In
6 445 addition, the data in this study is consistent with planktic foraminiferal concentrations from
7 446 the Barents Sea region (e.g. Klitgaard Kristensen *et al.* 2013; Duplessy *et al.* 2001). When
8 447 compared with other studies from the region (e.g. Zamelczyk *et al.* 2012, 2013; Berben *et al.*
9 448 2014), however, the current fragmentation and mean shell weight data indicate good
10 449 preservation, especially throughout the early part of the record. Therefore, the generally low
11 450 planktic foraminiferal concentrations are attributed here to the environmental conditions such
12 451 as the shallow shelf environment influenced by Arctic Water with a reduced salinity and the
13 452 proximity of the sea ice margin.

14
15
16 453 Regarding the planktic foraminiferal oxygen isotope signal, studies of recent foraminiferal
17 454 calcite and the isotopic composition of water masses by Lubinski *et al.* (2001) demonstrate
18 455 that, in the Barents Sea, these are controlled mainly by temperature changes rather than
19 456 salinity. However, the water masses in the region are also influenced by meltwater and
20 457 reduced salinities, especially during the earliest part of the Holocene, although this influence
21 458 probably diminished around ca. 11 000 cal a BP (Klitgaard Kristensen *et al.*, 2013).
22 459 Therefore, it is further assumed that the stable isotope record has been mainly controlled by
23 460 temperature.

24
25
26 461
27
28
29 462 *Period I (ca. 9500–5900 cal a BP): minimum sea ice conditions with reduced*
30 463 *SpSIC (ca. 25%)*

31
32
33
34
35
36
37
38
39
40
41
42 464 During Period I, low IP₂₅ concentrations reflect reduced seasonal sea ice, while high
43 465 brassicasterol and HBI III concentrations are indicative of open water and sea ice margin
44 466 conditions, respectively (Fig. 3a-c). At the same time, the lowest P_BIP₂₅ and P_{III}IP₂₅ values
45 467 indicate reduced spring sea ice conditions, with longer (warmer) summers suitable for
46 468 phytoplankton production (Müller *et al.*, 2011; Belt *et al.*, 2015; Smik *et al.*, 2016) (Fig. 3e-f),
47 469 which is also reflected by the generally higher TOC values (Fig. 3d). Maximum HBI III
48 470 concentrations indicate decreasing winter ice margin conditions from ca. 9500–8500 cal a BP
49 471 (Belt *et al.*, 2015), with SpSIC estimates consistently less than 50% (mean ca. 25%) (Fig. 3g)
50 472 and an absence of summer sea ice (Fig. 3f-g). The occurrence of reduced SpSIC and longer
51 473 (ice-free) summers is consistent with longer ice-free seasons and a retreated ice margin

1
2
3 474 observed in the northern Barents Sea (Duplessy *et al.*, 2001) and increased phytoplankton
4 475 production in the northern Fram Strait (Müller *et al.*, 2009, 2012) (for location of these study
5 476 sites please refer to Fig. 1). Reduced spring sea ice conditions likely indicate the occurrence
6 477 of the Holocene Thermal Maximum as recorded at the sea surface ca. 9300–6500 cal a BP.
7
8 478 The subsequent increase in IP₂₅ concentration after ca. 6500 cal a BP reflects a general
9 479 enhancement in sea ice conditions probably marking the gradual transition of the Holocene
10 480 Thermal Maximum towards Neoglacial conditions (Fig. 6b). Similar conclusions regarding
11 481 timing and termination of the Holocene Thermal Maximum based on IP₂₅ records have been
12 482 made for the Fram Strait (until ca. 8400 cal a BP; (Müller *et al.*, 2009)) and the West Svalbard
13 483 margin, where the last phase of the Holocene Thermal Maximum was recorded ca. 8500–
14 484 7000 cal a BP (Müller *et al.*, 2012). Furthermore, the observed disappearance of sea ice in the
15 485 western Barents Sea from ca. 10 700–7700 cal a BP has been linked previously to the
16 486 Holocene Thermal Maximum (Sarnthein *et al.*, 2003).

17
18 487 The light $\delta^{18}\text{O}$ (*N. pachyderma*) values ca. 8800–7300 cal a BP indicate a small temperature
19 488 rise, possibly reflecting a gradual shift towards a warmer sub-surface water mass due to
20 489 increased Atlantic Water inflow (Fig. 6e). The relatively light $\delta^{18}\text{O}$ values also coincide with
21 490 high insolation, thereby reflecting the Holocene Thermal Maximum at the core site (Fig. 6e).
22 491 The strong increase in $\delta^{18}\text{O}$ values ca. 7600–7300 cal a BP probably reflects its termination, a
23 492 conclusion consistent with observations of Duplessy *et al.* (2001) for a nearby location.
24 493 Furthermore, Hald *et al.* (2007) presented a time-transgressive Atlantic Water inflow from
25 494 south to north along the Norwegian and Svalbard margins. Risebrobakken *et al.* (2011)
26 495 suggested that this time-transgressive northward intensified heat advection resulted from
27 496 major reorganization of the ocean circulation following the deglaciation. Hence, throughout
28 497 the Holocene Thermal Maximum, high latitude radiative forcing was not responsible for the
29 498 overall conditions of the water column and ocean dynamics, although it might have further
30 499 enhanced the transport of warm salty water (Risebrobakken *et al.*, 2011). Within the broader
31 500 study area, Lubinski *et al.* (2001) associated decreasing $\delta^{18}\text{O}$ values ca. 10 000–6800 cal a BP
32 501 with a possible increase of surface water temperatures due to a return inflow of warm water.
33 502 A stronger Atlantic Water inflow delivered by the Svalbard Branch has also been recorded at
34 503 the western and northern Svalbard margins ca. 8000 cal a BP (Slubowska *et al.*, 2005; Werner
35 504 *et al.*, 2013) and in the Franz Victoria Trough ca. 7500 cal a BP (Duplessy *et al.*, 2001).
36 505 However, since the $\delta^{18}\text{O}$ values do not correspond to the observed time-transgressive pattern
37 506 of the Svalbard Branch, it is assumed that the core site was influenced by Atlantic Water

1
2
3 507 inflow entering the Barents Sea via the North Cape Current. This is consistent with decreased
4 508 $\delta^{18}\text{O}$ observations in the southern Barents Sea ca. 11 000–9800 cal a BP (Risebrobakken *et*
5 509 *al.*, 2010), the western Barents Sea ca. 10 000 cal a BP (Berben *et al.*, 2014) and the north-
6 510 western Barents Sea ca. 7000 cal a BP (Klitgaard Kristensen *et al.*, 2013) (for study locations
7
8
9
10 511 please refer to Fig. 1).

11
12 512 During Period I, the overall high relative abundances of *N. pachyderma*, in particular ca.
13 513 9500–7300 cal a BP, suggest a dominance of Arctic Water masses and cold conditions at the
14 514 study site (Volkman, 2000). However, from ca. 7300–5900 cal a BP, the increased
15 515 abundances of sub-polar species as well as of total planktic foraminifera indicate a
16 516 pronounced influence of relatively warm Atlantic Water inflow at the core site (Bé and
17 517 Tolderlund, 1971; Johannessen *et al.*, 1994; Carstens *et al.*, 1997) (Fig. 6f-g).
18 518 Correspondingly, elevated planktic foraminiferal concentrations were recorded in the north-
19 519 eastern Barents Sea and linked to an intrusion of Atlantic Water (Duplessy *et al.*, 2001).
20 520 Similar interpretations were made for the northern Barents Sea (Klitgaard Kristensen *et al.*,
21 521 2013) and the western Barents Sea (Sarnthein *et al.*, 2003; Berben *et al.*, 2014).

22
23
24
25
26
27
28
29
30 522 Nonetheless, the timing of changes in Atlantic Water inflow based on planktic foraminiferal
31 523 assemblages (ca. 7300–5900 cal a BP) differs from that based on $\delta^{18}\text{O}$ (ca. 8800–7300 cal a
32 524 BP). In the Arctic Ocean, the calcification of *N. pachyderma* is linked to phytoplankton
33 525 blooms occurring mainly in August (Kohfeld *et al.*, 1996; Volkman, 2000), whereas the
34 526 planktic foraminiferal fauna reflects an annual signal. Additionally, sea ice conditions can
35 527 result in a shift in the growing season (e.g. Farmer *et al.*, 2008) and a species-specific change
36 528 in its calcification depth. Therefore, the $\delta^{18}\text{O}$ of *N. pachyderma* reflects a different
37 529 temperature compared to the total foraminiferal assemblage (Simstich *et al.*, 2003) and might
38 530 reflect a different signal with respect to seasonality and/or water depth. Furthermore, the
39 531 faunal response depends on more factors than temperature and salinity. For example, *T.*
40 532 *quinqueloba* also depends on the available food supply (e.g. Volkman, 2000) and is
41 533 characteristic of Arctic Front conditions in the western Barents Sea (Burhol, 1994). An
42 534 increased nutrition availability associated with oceanic front conditions might have followed
43 535 later in time. Indeed, such a delay in food supply is suggested by increasing $\delta^{13}\text{C}$ values ca.
44 536 7300–5800 cal a BP which likely reflect enhanced primary production, possibly associated
45 537 with increased seasonal sea ice conditions, as suggested from the IP₂₅ data. Hence, the timing
46 538 of increased relative abundances of sub-polar species is probably related to a combination of
47
48
49
50
51
52
53
54
55
56
57
58
59
60

1
2
3 539 enhanced Atlantic Water inflow and increased nutrition availability, as seen previously in the
4 540 northern Barents Sea (Duplessy *et al.*, 2001).

5
6
7 541 For Period I, the new proxy data, combined with outcomes from previous studies, indicate
8 542 that the study site was characterized by reduced sea ice conditions during relatively short
9 543 spring seasons, enhanced phytoplankton production within the proximity of the sea ice
10 544 margin, and a winter sea ice margin in the proximity of the core site at ca. 78° N (Fig. 7a).
11
12 545 These sea surface conditions were likely influenced by maximum insolation, while the sub-
13 546 surface water masses were probably controlled more by oceanic dynamics (Andersson *et al.*,
14 547 2010; Risebrobakken *et al.*, 2011). In particular, a time-transgressive Atlantic Water inflow
15 548 resulted in initially cold water masses followed by warmer Atlantic Water at the study site.
16
17 549 The strengthening of Atlantic Water inflow might have additionally contributed to the
18 550 reduced sea ice conditions as seen during modern times in the Barents Sea (Årthun *et al.*,
19 551 2012). Such a proposed sea ice scenario implies that water masses south of the study area
20 552 were ice free, consistent with open water conditions observed in the western Barents Sea
21 553 (Sarnthein *et al.*, 2003; Berben *et al.*, 2014) and the West Svalbard margin (Müller *et al.*,
22 554 2012) (Fig. 7a) during the early Holocene.

23
24
25
26
27
28
29
30
31 555

32
33
34 556 *Period II (ca. 5900–2700 cal a BP): marginal ice zone conditions with*
35 557 *increasing SpSIC (ca. 60%)*

36
37
38 558 Throughout Period II, higher IP₂₅ concentrations and parallel decreases in brassicasterol and
39 559 HBI III concentrations reflect increased seasonal sea ice with less open water conditions (Fig.
40 560 3a-c). Increasing P_BIP₂₅ and P_{III}IP₂₅ values indicate marginal ice zone conditions at the study
41 561 site (Müller *et al.*, 2011; Belt *et al.*, 2015) (Fig. 3e-f) with a mean SpSIC of ca. 60% but
42 562 increasing throughout this interval to ca. 70% (Fig. 6d). Despite a general increase in SpSIC,
43 563 however, the P_{III}IP₂₅ data suggest that the site was probably ice free throughout the summer
44 564 months (Smik *et al.*, 2016) (Fig. 6c). Similar IP₂₅-based reconstructions of sea ice conditions
45 565 have been attributed to mid Holocene Neoglacial cooling for the northern Fram Strait (Müller
46 566 *et al.*, 2009) and the West Svalbard margin (Müller *et al.*, 2012).

47
48
49 567 The heavy $\delta^{18}\text{O}$ (*N. pachyderma*) values during Period II indicate lower temperatures and a
50 568 decreased influence of Atlantic Water (Fig. 6e), consistent with previous observations from
51 569 the region (Duplessy *et al.*, 2001; Klitgaard Kristensen *et al.*, 2013). It has also been

1
2
3 570 suggested that Arctic Water from the north-eastern Barents Sea might have influenced the
4 571 western Barents Sea due to less heat advection from the south (Hald *et al.*, 2007).

5
6
7 572 The dominance of *N. pachyderma*, along with decreased abundances of sub-polar
8 573 foraminifera, such as *T. quinqueloba* and *N. incompta* indicate the prevailing presence of
9 574 colder Arctic Water at the core site (Volkman, 2000) (Fig. 6f-g). This is consistent with
10 575 foraminifera-based observations of cold conditions after ca. 5200 cal a BP in the eastern Fram
11 576 Strait (Werner *et al.*, 2013) and reduced Atlantic Water inflow in the western Barents Sea
12 577 (Sarnthein *et al.*, 2003).

13
14
15
16
17
18 578 Combined, the biomarker and microfossil proxy data indicate a continuous cooling trend
19 579 during Period II with a dominance of cold Arctic Water and an accompanying increase in
20 580 SpSIC, likely as a result of decreasing summer insolation and a cooler surface water layer.
21 581 Consequently, the strongly reduced Atlantic Water inflow could not have affected the sea ice
22 582 conditions in the same way as was proposed for Period I. In addition, our data suggest that the
23 583 maximum winter sea ice margin was probably located ca. 76–77° N or, at least, further south
24 584 compared to the Period I (Fig. 7a-b). This is in good agreement with sea ice conditions at the
25 585 continental slope of western Svalbard (Müller *et al.*, 2012), although sea ice did not extend as
26 586 far as the western Barents Sea (Berben *et al.*, 2014) (Fig. 7b). With respect to the position of
27 587 the summer sea ice margin, the increased P_{III}IP₂₅ values also suggest a location further south
28 588 compared to Period I, consistent with previous observations in the northern Barents Sea after
29 589 ca. 6000 cal a BP (Duplessy *et al.*, 2001; Klitgaard Kristensen *et al.*, 2013) (Fig. 7b).

30
31
32
33
34
35
36
37
38
39 590

40
41 591 *Period III (ca. 2700 cal a BP–present): Arctic frontal conditions with high*
42 592 *SpSIC (ca. 75%) and summer sea ice*

43
44
45
46 593 Increases to IP₂₅, P_BIP₂₅ and P_{III}IP₂₅ reflect further increases in spring sea ice conditions
47 594 during Period III (Fig. 3a; e-f), while lower brassicasterol and HBI III concentrations indicate
48 595 less open water phytoplankton production consistent with lower TOC values (Fig. 3b-d).
49 596 These results point to Arctic frontal conditions that are similar to the modern setting (Müller
50 597 *et al.*, 2011; Belt *et al.*, 2015). Indeed, the P_{III}IP₂₅-based SpSIC estimates (ca. 75%) align
51 598 closely with contemporary values derived from satellite records (Smik *et al.*, 2016) (Fig. 6c-
52 599 d), while P_{III}IP₂₅ values generally >0.8 are also indicative of the occurrence of summer sea ice
53 600 (Smik *et al.*, 2016), also a feature of the modern setting. Consistent with these findings,

1
2
3 601 extended sea ice conditions have been reported for the Fram Strait for the last ca. 3000 cal a
4 602 BP (Müller *et al.*, 2012).

5
6
7 603 The mainly light, but variable, $\delta^{18}\text{O}$ (*N. pachyderma*) values, are most likely indicative of a
8 604 generally increased influence of Atlantic Water inflow (Fig. 6e), consistent with previous
9 605 reports of episodic increases in Atlantic Water for the northern Barents Sea (Duplessy *et al.*,
10 606 2001; Lubinski *et al.*, 2001), the western Barents Sea (Wilson *et al.*, 2011; Berben *et al.*,
11 607 2014) and the Svalbard margin (Jernas *et al.*, 2013; Werner *et al.*, 2013) during the late
12 608 Holocene.

13
14
15
16
17
18 609 The decrease in *N. pachyderma* and increased relative abundance of sub-polar foraminifera,
19 610 especially *G. bulloides*, which is usually associated with the warmest parts of the Norwegian
20 611 Atlantic Current (Johannessen *et al.*, 1994) also reflect the generally increasing influence of
21 612 Atlantic Water during this period (Fig. 6f-g). However, the fluctuations in the faunal data
22 613 throughout Period III still indicate variability in the influence of Atlantic Water consistent
23 614 with previous findings from the western Barents Sea (Sarnthein *et al.*, 2003).

24
25
26
27
28
29 615 The increase in sea ice conditions reflects an overall cooling trend recorded previously in
30 616 various Arctic terrestrial (e.g. Bjune *et al.*, 2009; Kaufman *et al.*, 2009), ice core (e.g.
31 617 Kaufman *et al.*, 2009; Divine *et al.*, 2011) and marine records (e.g. Slubowska *et al.*, 2005;
32 618 Skirbekk *et al.*, 2010), likely resulting from lower insolation affecting the sea surface. A
33 619 negative solar irradiance anomaly ca. 2850–2600 cal a BP may also have resulted in
34 620 decreased ventilation of the sub-surface waters, as corroborated by modelling experiments
35 621 (Renssen *et al.*, 2006). Meanwhile, the increased influence of Atlantic Water inflow might be
36 622 attributed to stronger stratification among the upper layers as seen in previous studies of the
37 623 Barents Sea (Lubinski *et al.*, 2001; Duplessy *et al.*, 2005; Risebrobakken *et al.*, 2010; Wilson
38 624 *et al.*, 2011) and the Svalbard margin (Jernas *et al.*, 2013; Werner *et al.*, 2013).

39
40
41
42
43
44
45
46 625 The occurrence of sea surface cooling and sub-surface warming indicates that Period III was
47 626 most likely characterized by a strong vertical stratification and a decoupling between the
48 627 atmosphere and the oceanic sub-surface. Summer insolation was at its lowest during Period
49 628 III (Fig. 6a), resulting in cooler atmospheric temperatures and potentially enhanced sea ice
50 629 production and/or reduced sea ice melt. In addition to the stronger vertical stratification of the
51 630 water column, the increased sea ice conditions probably also limited the heat exchange
52 631 between the atmosphere and the sub-surface water masses. In terms of seasonality, we suggest
53 632 that relatively long spring seasons with extensive sea ice conditions would have been
54
55
56
57
58
59
60

1
2
3 633 accompanied by shorter (and probably cooler) summers with lower phytoplankton production
4 634 (Fig. 7c). Overall, the site was characterized by extensive sea ice conditions (SpSIC typically
5 635 ca. 75%) with at least partial sea ice occurrence in the summer months (Fig. 7c). Such
6 636 interpretations are also consistent with previous qualitative reports of intensified sea ice
7 637 occurrence in the northern Barents Sea (Duplessy *et al.*, 2001; Klitgaard Kristensen *et al.*,
8 638 2013), increasing sea ice conditions in the Fram Strait (Müller *et al.*, 2009, 2012; Werner *et al.*,
9 639 2014) and in the western Barents Sea throughout the last ca. 1100 cal a BP (Berben *et al.*,
10 640 2014). Hence, the data suggest a south-westwards transgression of the sea ice margin (Fig.
11 641 7c). Finally, the sea ice conditions most likely exceeded the modern sea ice margin during the
12 642 (pre-industrial) late Holocene (Fig. 7c). A slight reversal in the extent of spring sea ice
13 643 conditions during recent decades and a return to more open water conditions during summer
14 644 (c.f. Period II) is evident during the last ca. 100 yr from observational records (Divine and
15 645 Dick, 2006).

646

647 **Conclusions**

648 Early to late Holocene semi-quantitative estimates of SpSIC and the qualitative occurrence of
649 summer sea ice in the northern Barents Sea have been reconstructed based on the variability
650 of source-specific biomarkers within a marine sediment core taken from the Olga Basin.
651 Additional proxy data based on planktic foraminifera that reflect the sub-surface water masses
652 have demonstrated the evolution of Atlantic Water inflow to the Barents Sea. The major
653 palaeoceanographic evolution can be summarised as follows: During Period I (ca. 9500–5900
654 cal a BP), reduced SpSIC (ca. 25%) was controlled, primarily, by relatively high summer
655 insolation. The core site was also influenced by Atlantic Water entering the Barents Sea via
656 the North Cape Current which caused an increased heat exchange between the ocean and the
657 atmosphere and likely contributed to reduced sea ice conditions. The site was probably
658 located close to the maximum winter sea ice margin, such that it experienced only relatively
659 short periods of sea ice during the spring together with long (ice-free) productive summers.

660 An overall cooling trend characterized Period II (ca. 5900–2700 cal a BP), with increased
661 SpSIC (ca. 60%) and delivery of cold Arctic Water. This interval was also characterized by a
662 general southward advance of the winter and summer sea ice margins, although, summer
663 months were still ice free.

1
2
3 664 Period III (ca. 2700 cal a BP–present) was marked by extensive SpSIC (ca. 75%), partial
4 665 summer sea ice occurrence and increased Atlantic Water inflow. Increased sea ice conditions
5 666 were probably induced by progressively lower insolation, while sub-surface warming due to
6 667 increased Atlantic Water demonstrates a likely decoupling between the atmosphere and the
7 668 ocean. The maximum winter sea ice margin was probably at its most southerly location within
8 669 the record, with long spring seasons of extensive sea ice conditions followed by shorter and
9 670 less productive summers. A slight retreat in the position of the winter sea ice margin is
10 671 proposed for recent decades based on observational records.
11
12
13
14
15
16
17
18
19

672

673 **Supporting information**

674 Additional supporting information related to this article may be found in the online version of
675 this article.

676 **Table S1.** CTD data presented in Fig. 1

677 **Table S2.** Age model presented in Fig. 2

678 **Table S3.** Biomarker data presented in Fig. 3

679 **Table S4.** Foraminiferal fauna data presented in Fig. 4

680 **Table S5.** Stable isotope data presented in Fig. 5

681

682 *Acknowledgements.* All data used in this work can be found in the supporting information for this paper. This
683 work was carried out within the framework of the Initial Training Network program “Changing Arctic and
684 Subarctic Environments” (CASE, Grant Agreement No. 238111) funded by the European Commission within
685 the 7th Framework Program People, the Research Council of Norway in addition to UiT–The Arctic University
686 of Norway and the Norwegian Polar Institute. Steffen Aagaard-Sørensen received financial support from the
687 GlaciBar (Glaciations in the Barents Sea area) project funded by the Norwegian Research Council (NRC grant
688 200672/S60), Statoil, Det Norske and BG Norge. Thanks are also extended to Trine Dahl and Julia Sen for
689 assisting with laboratory work in addition to Patricia Cabedo-Sanz for valuable discussions. Finally, we thank
690 Ruediger Stein and one anonymous reviewer for their constructive feedback improving this manuscript.

691

692 **References**

- 693 Abrahamsen E, Østerhus S, Gammelsrød T. 2006. Ice draft and current measurements from
694 the north-western Barents Sea, 1993-96. *Polar Research* **25**: 25-37.
- 695 Aksenov Y, Bacon S, Coward AC, Nurser AJG. 2010. The North Atlantic inflow to the Arctic
696 Ocean: high-resolution model study. *Journal of Marine Systems* **79**: 1-22.
- 697 Aksu AE, Vilks G. 1988. Stable isotopes in planktonic and benthic foraminifera from Arctic
698 Ocean surface sediments. *Canadian Journal of Earth Sciences* **25**: 701-709.
- 699 Andersson C, Pausata FSR, Jansen E, Risebrobakken B, Telford RJ. 2010. Holocene trends in
700 the foraminifer record from the Norwegian Sea and the North Atlantic Ocean. *Climate of the
701 Past* **6**: 179-193.
- 702 Barker S, Elderfield H. 2002. Foraminiferal calcification response to glacial interglacial
703 changes in atmospheric CO₂. *Science* **297**: 883-836.
- 704 Barker S, Kiefer T, Elderfield H. 2004. Temporal changes in North Atlantic circulation
705 constrained by planktonic foraminiferal shell weights. *Paleoceanography* **19**: PA3008.
- 706 Bauch D, Carstens J, Wefer G. 1997. Oxygen isotope composition of living
707 *Neogloboquadrina pachyderma* (sin.) in the Arctic Ocean. *Earth and Planetary Science
708 Letters* **146**: 47-58.
- 709 Bauch D, Carstens J, Wefer G, Thiede J. 2000. The imprint of anthropogenic CO₂ in the
710 Arctic Ocean: evidence from planktic d¹³C data from water column and sediment surfaces.
711 *Deep-Sea Research Pt. II* **9-11**: 1791-1808.
- 712 Bé AWH, Tolderlund DS. 1971. Distribution and ecology of living planktonic foraminifera in
713 surface waters of the Atlantic and Indian Oceans. In *The micropaleontology of oceans*, Funnel
714 BM, Riedel WR (eds). Cambridge University Press: London; 105-149.
- 715 Belt ST, Massé G, Rowland SJ, Poulin M, Michel C, LeBlanc B. 2007. A novel chemical
716 fossil of palaeo sea ice: IP₂₅. *Organic Geochemistry* **38**: 16-27.
- 717 Belt ST, Vare LL, Massé G, Manners HR, Price JC, MacLachlan SE, Andrews JT, Schmidt S.
718 2010. Striking similarities in temporal changes to spring sea ice occurrence across the central
719 Canadian Arctic Archipelago over the last 7000 years. *Quaternary Science Reviews* **29**: 3489-
720 3504.
- 721 Belt ST, Brown TA, Navarro Rodriguez A, Cabedo Sanz P, Tonkin A, Ingle R. 2012. A
722 reproducible method for the extraction, identification and quantification of the Arctic sea ice
723 proxy IP₂₅ from marine sediments. *Analytical Methods* **4**: 705-713.
- 724 Belt ST, Müller J. 2013. The Arctic sea ice biomarker IP₂₅: a review of current understanding,
725 recommendations for future research and applications in palaeo sea ice reconstructions.
726 *Quaternary Science Reviews* **79**: 9-25.
- 727 Belt ST, Cabedo-Sanz P, Smik L, Navarro-Rodriguez A, Berben SMP, Knies J, Husum K.
728 2015. Identification of paleo Arctic winter sea ice limits and the marginal ice zone: Optimised
729 biomarker-based reconstructions of late Quaternary Arctic sea ice. *Earth and Planetary
730 Science Letters* **431**: 127-139.

- 1
2
3 731 Berben SMP. 2014. *A Holocene palaeoceanographic multi-proxy study on the variability of*
4 732 *Atlantic water inflow and sea ice distribution along the pathway of Atlantic water*. The Arctic
5 733 University of Norway (PhD thesis).
6
7 734 Berben SMP, Husum K, Cabedo-Sanz P, Belt ST. 2014. Holocene sub-centennial evolution of
8 735 Atlantic water inflow and sea ice distribution in the western Barents Sea. *Climate of the Past*
9 736 **10**: 181-198.
10
11 737 Berger A. 1978. Long-term variations of daily insolation and quaternary climatic changes.
12 738 *Journal of Atmospheric Sciences* **35**: 2363-2367.
13
14 739 Birgel D, Stein R. 2004. Northern Fram Strait and Yermak Plateau: Distribution, variability
15 740 and burial of organic carbon and paleoenvironmental implications. In *The organic carbon*
16 741 *cycle in the Arctic Ocean*, Stein R, Macdonald RW (eds). Springer-Verlag: Berlin; 279-295.
17
18 742 Birgel D, Stein R, Hefter J. 2004. Aliphatic lipids in recent sediments of the Fram
19 743 Strait/Yermak Plateau (Arctic Ocean): composition, sources and transport processes. *Marine*
20 744 *Chemistry* **88**: 127-160.
21
22 745 Bjune AE, Seppä H, Birks HJB. 2009. Quantitative summer temperature reconstructions for
23 746 the last 2000 years based on pollen-stratigraphical data from northern Fennoscandia. *Journal*
24 747 *of Paleolimnology* **41**: 43-56.
25
26 748 Broecker WS, Clark E. 2001. An evaluation of Lohmann's foraminifera weight dissolution
27 749 index. *Paleoceanography* **16**: 531-534.
28
29 750 Brown TA, Belt ST, Philippe B, Mundy CJ, Massé G, Poulin M, Gosselin M. 2011. Temporal
30 751 and vertical variations of lipid biomarkers during a bottom ice diatom bloom in the Canadian
31 752 Beaufort Sea: Further evidence for the use of the IP₂₅ biomarker as a proxy for spring Arctic
32 753 sea ice. *Polar Biology* **34**: 1857-1868.
33
34 754 Brown TA, Belt ST. 2012. Identification of the sea ice diatom biomarker IP₂₅ in Arctic
35 755 benthic macrofauna: Direct evidence for a sea ice diatom diet in Arctic heterotrophs. *Polar*
36 756 *Biology* **35**: 131-137.
37
38 757 Brown TA, Belt ST, Tatarek A, Mundy CJ. 2014. Source identification of the Arctic sea ice
39 758 proxy IP₂₅. *Nature Communications* **5**: 4197.
40
41 759 Burhol ALS. 1994. *Recent distribution of planktonic foraminifera on the Svalbard-Barents*
42 760 *margin*. University of Tromsø (Master thesis).
43
44 761 Cabedo-Sanz P, Belt ST, Knies J, Husum K. 2013. Identification of contrasting seasonal sea
45 762 ice conditions during the Younger Dryas. *Quaternary Science Reviews* **79**: 74-86.
46
47 763 Cabedo-Sanz P, Belt ST. 2016a. Seasonal sea ice variability in eastern Fram Strait over the
48 764 last 2000 years. *Arktos* **2(22)**: 1-12.
49
50 765 Cabedo-Sanz P, Belt ST, Jennings AE, Andrews JT, Geirsdóttir Á. 2016b. Variability in drift
51 766 ice export from the Arctic Ocean to the North Icelandic Shelf over the last 8,000 years: a
52 767 multi proxy evaluation. *Quaternary Science Reviews* **146**: 99-115.
53
54 768 Carmack E, Barber D, Christensen J, Macdonald R, Rudels B, Sakshaug E. 2006. Climate
55 769 variability and physical forcing of the food webs and the carbon budget on panarctic shelves.
56 770 *Progress in Oceanography* **71**: 145-181.
57
58
59
60

- 1
2
3 771 Carstens J, Hebbeln D, Wefer G. 1997. Distribution of planktic foraminifera at the ice margin
4 772 in the Arctic (Fram Strait). *Marine Micropaleontology* **29**: 257-269.
5
6 773 Cifelli R. 1961. Globigerina incompta, a new species of pelagic foraminifera from the North
7 774 Atlantic. *Contributions Cushman Foundation Foraminiferal Research* **12**: 83-86.
8
9 775 Conan SMH, Ivanova EM, Brummer G-JA. 2002. Quantifying carbonate dissolution and
10 776 calibration of foraminiferal dissolution indices in the Somali Basin. *Marine Geology* **182**:
11 777 325-349.
12
13 778 Darling KF, Kucera M, Kroon D, Wade CM. 2006. A resolution for the coiling direction
14 779 paradox in Neogloboquadrina pachyderma. *Paleoceanography* **21**: PA2011.
15
16 780 Divine DV, Dick C. 2006. Historical variability of sea ice edge position in the Nordic Seas.
17 781 *Journal Geophysical Research* **111**: C01001.
18
19 782 Divine D, Isaksson E, Martma T, Meijer HAJ, Moore J, Pohjola V, van de Wal RSW,
20 783 Godtliobsen F. 2011. Thousand years of winter surface air temperature variations in Svalbard
21 784 and northern Norway reconstructed from ice-core data. *Polar Research* **30**: 7379.
22
23 785 Donner B, Wefer G. 1994. Flux and stable isotope composition of Neogloboquadrina
24 786 pachyderma and other planktonic foraminifers in the Southern Ocean (Atlantic sector). *Deep-*
25 787 *Sea Research Pt. I* **41**: 1733-1743.
26
27 788 Duplessy JC, Ivanova E, Murdmaa I, Paterne M, Labeyrie L. 2001. Holocene
28 789 paleoceanography of the northern Barents Sea and variations of the northward heat transport
29 790 by the Atlantic Ocean. *Boreas* **30**: 2-16.
30
31 791 Duplessy JC, Cortijo E, Ivanova E, Khusid T, Labeyrie L, Levitan M, Murdmaa I, Paterne M.
32 792 2005. Paleoceanography of the Barents Sea during the Holocene. *Paleoceanography* **20**:
33 793 A4004.
34
35 794 Ellingsen I, Slagstad D, Sundfjord A. 2009. Modification of water masses in the Barents Sea
36 795 and its coupling to ice dynamics: A model study. *Ocean Dynamics* **59**: 1095-1108.
37
38 796 Fahl K, Stein R. 2012. Modern seasonal variability and deglacial/Holocene change of central
39 797 Arctic Ocean sea ice cover: New insights from biomarker proxy records. *Earth Planetary*
40 798 *Science Letters* **351-352**: 123-133.
41
42 799 Fairbanks RG. 1989. A 17 000-year glacia-eustatic sea level record: Influence of glacial
43 800 melting rates on the Younger Dryas event and deep-ocean circulation. *Nature* **342**: 637-642.
44
45 801 Farmer EJ, Chapman MR, Andrews JE. 2008. Centennial-scale Holocene North Atlantic
46 802 surface temperatures from Mg/Ca ratios in Globigerina bulloides. *Geochemistry, Geophysics,*
47 803 *Geosystems* **9**: Q12029.
48
49 804 Forcino FL. 2012. Multivariate assessment of the required sample size for community
50 805 paleoecological research. *Palaeogeography, Palaeoclimatology, Palaeoecology* **315-316**:
51 806 134-141.
52
53 807 Gammelsrød T, Leikvin Ø, Lien V, Budgell WP, Loeng H, Maslowski W. 2009. Mass and
54 808 heat transports in the NE Barents Sea: Observations and models. *Journal of Marine Systems*
55 809 **75**: 56-69.
56
57
58
59
60

- 1
2
3 810 Hald M, Andersson C, Ebbesen H, Jansen E, Klitegaard-Kristensen D, Risebrobakken B,
4 811 Salomonsen GR, Sejrup HP, Sarnthein M, Telford R. 2007. Variations in temperature and
5 812 extent of Atlantic water in the northern North Atlantic during the Holocene. *Quaternary*
6 813 *Science Reviews* **26**: 3423-3440.
- 8 814 Hebbeln D, Henrich R, Baumann KH. 1998. Paleoceanography of the last glacial/interglacial
9 815 cycle in the Polar North Atlantic. *Quaternary Science Reviews* **17**: 125-153.
- 11 816 Henrich R, Baumann KH, Huber R, Meggers H. 2002. Carbonate preservation records of the
12 817 past 3 Myr in the Norwegian-Greenland Sea and the northern North Atlantic: Implications for
13 818 the history of NADW production. *Marine Geology* **184**: 17-39.
- 15 819 Hopkins TS. 1991. The GIN Sea: A synthesis of its physical oceanography and literature
16 820 review, 1972–1985. *Earth-Science Reviews* **30**: 175-318.
- 18 821 Ivanov VV, Alexeev VA, Repina I, Koldunov NV, Smirnov A. 2012. Tracing Atlantic water
19 822 signature in the Arctic Sea ice cover East of Svalbard. *Advances in Meteorology* **2012**:
20 823 201818, 11.
- 22 824 Jakobsson M, Grantz A, Kristoffersen Y, Macnab R. 2004. Physiography and bathymetry of
23 825 the Arctic Ocean. In *The Organic Carbon Cycle in the Arctic Ocean*, Stein R, Macdonald RW
24 826 (eds). Springer: New York; 1-5.
- 26 827 Jernas P, Klitgaard Kristensen D, Husum K, Wilson L, Koç N. 2013. Palaeoenvironmental
27 828 changes of the last two millennia on the western and northern Svalbard shelf. *Boreas* **42**: 236-
28 829 255.
- 30 830 Johannessen T, Jansen E, Flatøy A, Ravelo AC. 1994. The relationship between surface water
31 831 masses, oceanographic fronts and plaeoclimatic proxies in surface sediments of the
32 832 Greenland, Iceland, Norwegian Seas. In *Carbon Cycling in the Glacial Ocean: Constraints of*
33 833 *the Ocean's Role in Global Change*, Zahn R, Pedersen TF, Kaminski MA, Labeyrie L (eds).
34 834 Springer: Berlin, 61-86.
- 36 835 Jonkers L, Brummer G-JA, Peeters FJC, van Aken HM, De Jong MF. 2010. Seasonal
37 836 stratification, shell flux, and oxygen isotope dynamics of left-coiling *N. pachyderma* and *T.*
38 837 *quinqueloba* in the western sub polar North Atlantic. *Paleoceanography* **25**: PA2204.
- 40 838 Katz ME, Cramer BS, Franzese A, Hönisch B, Miller KG, Rosenthal Y, Wright J. 2010.
41 839 Traditional and emerging geochemical proxies in foraminifera. *Journal of Foraminiferal*
42 840 *research* **40(2)**:165-192.
- 44 841 Kaufman D, Ager TA, Anderson NJ, Anderson PM, Andrews JT, Bartlein PJ, Brubakker LB,
45 842 Coats LL, Cwynar LC, Duvall ML, Dyke AS, Edwards ME, Eisner WR, Gajewski K,
46 843 Geirsdottir A, Hu FS, Jennings AE, Kaplan MR, Kerwin MW, Loshkin AV, MacDonald GM,
47 844 Miller GH, Mock CJ, Oswald WW, Otto-Bliesner BL, Porinchu DF, Rühland K, Smol JP,
48 845 Steig EJ, Wolfe BB. 2004. Holocene thermal maximum in the western Arctic (0 - 180 °N).
49 846 *Quaternary Science Reviews* **23**: 529-560.
- 51 847 Kaufman DS, Schneider DP, McKay NP, Ammann CM, Bradley RS, Briffa KR, Miller GH,
52 848 Otto-Bliesner BL, Overpeck JT, Vinther BM. 2009. Recent warming reverses long-term arctic
53 849 cooling. *Science* **325(5945)**: 1236-1239.
- 55 850 Keigwin LD, Boyle EA. 1989. Late Quaternary paleochemistry of high-latitude surface
56 851 waters. *Palaeogeography, Palaeoclimatology, Palaeoecology* **73**: 85-106.

- 1
2
3 852 Klitgaard Kristensen D, Rasmussen TL, Koç N. 2013. Paleoceanographic changes in the
4 853 northern Barents Sea during the last 16 000 years – new constraints on the last deglaciation of
5 854 the Svalbard-Barents Ice Sheet. *Boreas* **42**: 798-813.
- 6
7 855 Knies J, Cabedo-Sanz P, Bel, ST, Baranwal S, Fietz S, Rosell-Melé A. 2014. The emergence of
8 856 modern sea ice cover in the Arctic Ocean. *Nature Communications* **5**: 5608.
- 9
10 857 Knudsen KL. 1998. Foraminiferer i Kvartær stratigrafi: Laboratorie og fremstillingsteknik
11 858 samt udvalgte eksempler. *Geologisk Tidsskrift* **3**: 1-25.
- 12
13 859 Koç N, Jansen E, Haflidason H. 1993. Paleoceanographic reconstructions of surface ocean
14 860 conditions in the Greenland, Iceland and Norwegian seas through the last 14 ka based on
15 861 diatoms. *Quaternary Science Reviews* **12**: 115-140
- 16
17 862 Kohfeld KE, Fairbanks RG, Smith SL. 1996. *Neogloboquadrina pachyderma* (sinistral
18 863 coiling) as paleoceanographic tracers in polar oceans: Evidence from northeast water polynya
19 864 plankton tows, sediments traps, and surface sediments. *Paleoceanography* **11**: 679-699.
- 20
21 865 Kwok R. 2009. Outflow of Arctic Ocean sea ice into the Greenland and Barents Seas: 1979-
22 866 2007. *Journal of Climate* **22(9)**: 2438-2457.
- 23
24 867 Kwok R, Maslowski W, Laxon S. 2005. On large outflows of Arctic sea-ice into the Barents
25 868 Sea. *Geophysical Research Letters* **32**: L22503.
- 26
27 869 Laskar J, Robutel P, Joutel F, Gastineau M, Correia ACM, Levrard B. 2004. A long-term
28 870 numerical solution for the insolation quantities of the Earth. *Astronomy and Astrophysics* **428**:
29 871 261-285.
- 30
31 872 Loeng H. 1991. Features of the physical oceanographic conditions of the Barents Sea. *Polar*
32 873 *Research* **10**: 5-18.
- 33
34 874 Loeng H, Ozhigin V, Ådlandsvik B, Sagen H. 1993. *Current Measurements in the*
35 875 *northeastern Barents Sea*, International Council for the Exploration of the Sea, Council
36 876 Meeting 1993/C:41, Hydrographic Committee; 22.
- 37
38 877 Lubinski DJ, Polyak L, Forman SL. 2001. Freshwater and Atlantic water inflows to the deep
39 878 northern Barents and Kara seas since ca 13 ¹⁴Cka: foraminifera and stable isotopes.
40 879 *Quaternary Science Reviews* **20**: 1851-1879.
- 41
42 880 Mangerud J, Bondevik S, Gulliksen S, Hufthammer AK, Høisæter T. 2006. Marine ¹⁴C
43 881 reservoir ages for 19th century whales and molluscs from the North Atlantic. *Quaternary*
44 882 *Science Reviews* **25**: 3228-3245.
- 45
46 883 Manley TO. 1995. Branching of Atlantic Water within the Greenland-Spitsbergen Passage:
47 884 An estimate of recirculation. *Journal of Geophysical Research* **100**: 20627-20634.
- 48
49 885 Massé G, Rowland SJ, Sicre M-A, Jacob J, Jansen E, Belt ST. 2008. Abrupt climate changes
50 886 for Iceland during the last millennium: Evidence from high resolution sea ice reconstructions.
51 887 *Earth and Planetary Science Letters* **269**: 565-569.
- 52
53 888 Méheust M, Fahl K, Stein R. 2013. Variability in modern sea surface temperature, sea ice and
54 889 terrigenous input in the sub-polar North Pacific and Bering Sea: Reconstruction from
55 890 biomarker data. *Organic Geochemistry* **57**: 54-64.
- 56
57
58
59
60

- 1
2
3 891 Méheust M, Stein R, Fahl K, Max L, Riethdorf J-R. 2015. High-resolution IP₂₅-based
4 892 reconstruction of sea ice variability in the western North Pacific and Bering Sea during the
5 893 past 18,000 years. *GeoMarine Letters* **36**: 101-111.
6
7 894 Midttun L. 1985. Formation of dense bottom water in the Barents Sea. *Deep-Sea Research*
8 895 **32**: 1233-1241.
9
10 896 Müller J, Massé G, Stein R, Belt ST. 2009. Variability of sea ice conditions in the Fram Strait
11 897 over the past 30000 years. *Nature Geoscience* **2(11)**: 772-776.
12
13 898 Müller J, Wagner A, Fahl K, Stein R, Prange M, Lohman G. 2011. Towards quantitative sea
14 899 ice reconstructions in the northern North Atlantic: A combined biomarker and numerical
15 900 modelling approach. *Earth and Planetary Science Letters* **306**: 137-148.
16
17 901 Müller J, Werner K, Stein R, Fahl K, Moros M, Jansen E. 2012. Holocene cooling culminates
18 902 in sea ice oscillations in Fram Strait. *Quaternary Science Reviews* **47**: 1-14.
19
20 903 Müller J, Stein R. 2014. High-resolution record of late glacial sea ice changes in Fram Strait
21 904 corroborates ice-ocean interactions during abrupt climate shifts. *Earth and Planetary Science*
22 905 *Letters* **403**: 446-455.
23
24 906 National Snow and Ice Data Center (NSIDC), Boulder Colorado, www.nsidc.com
25
26 907 Navarro-Rodriguez A, Belt ST, Knies J, Brown TA. 2013. Mapping recent sea ice conditions
27 908 in the Barents Sea using the proxy biomarker IP₂₅: Implications for palaeo sea ice
28 909 reconstructions. *Quaternary Science Reviews* **79**: 26-39.
29
30 910 Novitskiy VP. 1961. Permanent currents of the northern Barents Sea. *Trudy*
31 911 *Gosudarstvennogo Okeanograficheskogo Instituta* **64**: 1-32. (English Translation).
32
33 912 Oppo DW, Fairbanks RG. 1989. Carbon isotope composition of tropical surface water during
34 913 the past 22,000 years. *Paleoceanography* **4**: 333-351.
35
36 914 Pados T, Spielhagen RF. 2014. Species distribution and depth habitat of recent planktic
37 915 foraminifera in Fram Strait, Arctic Ocean. *Polar Research* **33**: 22483.
38
39 916 Pfirman SL, Bauch D, Gammelsrød T. 1994. The Northern Barents Sea: water mass
40 917 distribution and modification. In *The Polar Oceans and Their Role in Shaping the Global*
41 918 *Environment*, Johannessen OM, Muench RD, Overland JE (eds). *AGU Geoph. Monog.*
42 919 *Series.*, **85**: 77-94.
43
44 920 Pfuhl HA, Shackleton NJ. 2004. Two proximal, high-resolution records of foraminiferal
45 921 fragmentation and their implications for changes in dissolution. *Deep-Sea Research Pt. I* **51**:
46 922 809-832.
47
48 923 Polyak L, Belt ST, Cabedo-Sanz P, Yamamoto M, Park YH. 2016. Holocene sea-ice
49 924 conditions and circulation at the Chukchi-Alaskan margin, Arctic Ocean, inferred from
50 925 biomarker proxies. *The Holocene* **26**: 1810-1821.
51
52 926 Rasmussen TL, Thomsen E, Slubowska MA, Jessen S, Solheim A, Koç N. 2007.
53 927 Paleocceanographic evolution of the SW Svalbard margin (76 °N) since 20 000 ¹⁴C yr BP.
54 928 *Quaternary Research* **67**: 100-114.
55
56
57
58
59
60

- 1
2
3 929 Reimer PJ, Baillie MGL, Bard E, Bayliss A, Beck JW, Blackwell PG, Ramsey CB, Buck CE,
4 930 Burr GS, Edwards RL, Friedrich HM, Grootes PM, Guilderson TP, Hajdas I, Heaton TJ,
5 931 Hogg AG, Hughen KA, Kaiser KF, Kromer B, McCormac FG, Manning SW, Reimer RW,
6 932 Richards DA, Southon JR, Talamo S, Turney CSM, Van Der Plicht J, Weyhenmeyer CE.
7 933 2009. IntCal09 and Marine09 radiocarbon age calibration curves, 0-50 000 years cal BP.
8 934 *Radiocarbon* **51**: 1111-1150.
- 9
10 935 Renssen H, Goosse H, Muscheler R. 2006. Coupled climate model simulation of Holocene
11 936 cooling events: oceanic feedback amplifies solar forcing. *Climate of the Past* **2**: 79-90.
- 12
13 937 Risebrobakken B, Morros M, Ivanova EV, Chistyakova N, Rosenberg R. 2010. Climate and
14 938 oceanographic variability in the SW Barents Sea during the Holocene. *The Holocene* **20**: 609-
15 939 621.
- 16
17 940 Risebrobakken B, Dokken T, Smedsrud LH, Andersson C, Jansen E, Moros M, Ivanova EV.
18 941 2011. Early Holocene temperature variability in the Nordic Seas: The role of oceanic heat
19 942 advection versus changes in orbital forcing. *Paleoceanography* **26**: PA4206.
- 20
21 943 Rudels B. 1987. On the mass balance of the Polar Ocean, with special emphasis on the Fram
22 944 Strait. *Norsk Polarinstitutt Skrifter* **188**: 53.
- 23
24 945 Rudels B, Korhonen M, Schauer U, Pisarev S, Rabe B, Wisotzki A. 2014. Circulation and
25 946 transformation of Atlantic water in the Eurasian Basin and the contribution of the Fram Strait
26 947 inflow branch to the Arctic Ocean heat budget. *Progress in Oceanography* **132**: 128-152.
- 27
28 948 Sakshaug E, Bjørge A, Gulliksen B, Loeng H, Mehlum F. 1992. *Økosystem Barentshavet*.
29 949 Norges Allmennevitenskapelige Forskningsråd, Norges Fiskeriforskningsråd,
30 950 Miljøverndepartementet, 304.
- 31
32 951 Sarnthein M, Van Kreveld S, Erlenkeuser H, Grootes PM, Kucera M, Pflaumann U, Schulz
33 952 M. 2003. Centennial-to-millennial-scale periodicities of Holocene climate and sediment
34 953 injections off the western Barents shelf, 75 °N. *Boreas* **32**: 447-461.
- 35
36 954 Schauer U, Loeng H, Rudels B, Ozhigin VK, Dieck W. 2002. Atlantic Water flow through the
37 955 Barents and Kara Seas. *Deep-Sea Research Pt. I* **49**: 2281-2298.
- 38
39 956 Screen JA, Simmonds I. 2010. The central role of diminishing sea ice in recent Arctic
40 957 temperature amplification. *Nature* **464**: 1334-1337.
- 41
42 958 Serreze MC, Francis JA. 2006. The arctic amplification debate. *Climate Change* **76(3-4)**: 241-
43 959 264.
- 44
45 960 Serreze M, Barrett A, Slater A, Steele M, Zhang J, Tenberth K. 2007. The large-scale energy
46 961 budget of the Arctic. *Journal of Geophysical Research* **112**: D11122.
- 47
48 962 Shimada K, Kamoshida T, Itoh M, Nishino S, Carmack E, McLaughlin F, Zimmermann S,
49 963 Proshutinsky A. 2006. Pacific Ocean inflow: Influence on catastrophic reduction of sea ice
50 964 cover in the Arctic Ocean. *Geophysical Research Letters* **33**: L08605
- 51
52 965 Simstich J, Sarnthein M, Erlenkeuser H. 2003. Paired $\delta^{18}\text{O}$ signals of *N. pachyderma* (s) and
53 966 *T. quinqueloba* show thermal stratification structure in the Nordic Seas. *Marine*
54 967 *Micropaleontology* **48**: 107-125.
- 55
56
57
58
59
60

- 1
2
3 968 Skirbekk K, Klitgaard Kristensen D, Rasmussen TL, Koç N, Forwick M. 2010. Holocene
4 969 climate variations at the entrance to a warm Arctic fjord: evidence from Kongsfjorden trough,
5 970 Svalbard. *Geological society, London, Special Publications 2010* **344**: 289-304.
- 6
7 971 Slubowska MA, Koç N, Rasmussen TL, Klitgaard-Kristensen D. 2005. Changes in the flow
8 972 of Atlantic water into the Arctic Ocean since the last deglaciation: Evidence from the northern
9 973 Svalbard continental margin, 80N. *Paleoceanography* **20**: PA4014.
- 10
11 974 Smedsrud LH, Esau I, Ingvaldsen RB, Eldevik T, Haugan PM, Li C, Lien VS, Olsen A, Omar
12 975 AM, Otterå OH, Risebrobakken B, Sandø AB, Semenov VA, Sorokina SA. 2013. The role of
13 976 the Barents Sea in the Arctic climate system. *Reviews of Geophysics* **51(3)**: 415-449.
- 14
15 977 Smik L, Cabedo-Sanz P, Belt ST. 2016. Semi-quantitative estimates of paleo Arctic sea ice
16 978 concentration based on source-specific highly branched isoprenoid alkenes: A further
17 979 development of the PIP25 index. *Organic Geochemistry* **92**: 63-69.
- 18
19 980 Smith WO, Sakshaug E. 1990. Polar phytoplankton. In *Polar oceanography, Part B:*
20 981 *Chemistry, Biology and Geology*, Smith WO (ed). Academic Press: New York; 447-525.
- 21
22 982 Sorteberg A, Kvingedal B. 2006. Atmospheric forcing on the Barents Sea winter ice extent.
23 983 *Journal of Climate* **19**: 4772-4784.
- 24
25 984 Spielhagen RF, Erlenkeuser H. 1994. Stable oxygen and carbon isotopes in planktic
26 985 foraminifera from the Arctic Ocean surface sediments: Reflection of the low salinity surface
27 986 water layer. *Marine Geology* **119**:227-250.
- 28
29 987 Spielhagen RF, Werner K, Aagaard-Sørensen S, Zamelczyk K, Kandiano E, Budeus G,
30 988 Husum K, Marchitto T, Hald M. 2011. Enhanced modern heat transfer to the Arctic by warm
31 989 Atlantic water. *Science* **331**: 450-453.
- 32
33 990 Stangeew E. 2001. *Distribution and isotopic composition of living planktonic foraminifera N.*
34 991 *pachyderma (sinistral) and T. quinqueloba in the high latitude North Atlantic*. Ph.D. thesis,
35 992 Math.-Naturwiss. Fak., Christian-Albrechts-Univ., Kiel, Germany. (Available at [http://e-](http://e-diss.uni-kiel.de/diss_464/pp)
36 993 [diss.uni-kiel.de/diss_464/pp](http://e-diss.uni-kiel.de/diss_464/pp)).
- 37
38 994 Stein R, Fahl K, Schade I, Manerung A, Wassmuth S, Niessen F, Nam S. 2016a. Holocene
39 995 variability in sea ice cover, primary production, and Pacific-Water inflow and climate change
40 996 in the Chukchi and East Siberian Seas (Arctic Ocean). *Journal of Quaternary Science* ISSN
41 997 0267-8179, DOI:10.1002/jqs.2929.
- 42
43 998 Stein R, Fahl K, Schreck M, Knorr G, Niessen F, Forwick M, Gebhardt C, Jensen L,
44 999 Kaminski M, Kopf A, Matthiessen J, Jokat W, Lohmann G. 2016b. Evidence for ice-free
45 1000 summers in the late Miocene central Arctic Ocean. *Nature Communications* **7**: 11148.
- 46
47 1001 Steinsund PI, Hald M. 1994. Recent carbonate dissolution in the Barents Sea:
48 1002 Paleooceanographic applications. *Marine Geology* **117**: 303-316.
- 49
50 1003 Stroeve J, Holland MM, Meier W, Scambos T, Serreze M. 2007. Arctic sea ice decline: Faster
51 1004 than forecast. *Geophysical Research Letters* **34**:L09501.
- 52
53 1005 Stroeve J, Serreze MC, Holland MM, Kay JE, Malanik J, Barrett AP. 2012. The Arctic's
54 1006 rapidly shrinking sea ice cover: a research synthesis. *Climate Change* **110**:1005-1027.
- 55
56
57
58
59
60

- 1
2
3 1007 Stuiver M, Reimer PJ. 1993. Extended ^{14}C data base and revised CALIB 3.0 ^{14}C age
4 1008 calibration program. *Radiocarbon* **35**: 215-230.
- 5
6 1009 Vare LL, Massé G, Gregory TR, Smart CW, Belt ST. 2009. Sea ice variations in the central
7 1010 Canadian Arctic Archipelago during the Holocene. *Quaternary Science Reviews* **28**: 1354-
8 1011 1366.
- 9
10 1012 Vare LL, Massé G, Belt ST. 2010. A biomarker-based reconstruction of sea ice conditions for
11 1013 the Barents Sea in recent centuries. *The Holocene* **20(4)**: 637-643.
- 12
13 1014 Vinje TE. 1977. Sea ice conditions in the European sector of the marginal seas of the Arctic,
14 1015 1966-75. *Arbok Norsk Polarinstitut* **1975**: 163-174.
- 15
16 1016 Vinje T. 2001. Anomalies and trends of sea ice extent and atmospheric circulation in the
17 1017 Nordic Seas during the period 1864-1998. *Journal of Climate* **14(3)**: 255-267.
- 18
19 1018 Volkman R. 2000. Planktic foraminifers in the outer Laptev Sea and the Fram Strait: Modern
20 1019 distribution and ecology. *Journal Foraminiferal Research* **30**: 157-176.
- 21
22 1020 Wassmann P, Reigstad M, Haug T, Rudels B, Carroll ML, Hop H, Gabrielsen GW, Falk-
23 1021 Petersen S, Denisenko SG, Arashkevich E, Slagstad D, Pavlova O. 2006. Food webs and
24 1022 carbon flux in the Barents Sea. *Progress in Oceanography* **71**: 232-287.
- 25
26 1023 Wassmann P. 2011. Arctic marine ecosystems in an era of rapid climate change. *Progress in*
27 1024 *Oceanography* **90**: 1-17.
- 28
29 1025 Weckström K, Massé G, Collins LG, Hanhijärvi S, Bouloubassi I, Sicre M-A, Seidenkrantz
30 1026 M-S, Schmidt S, Andersen TJ, Andersen ML, Hill B, Kuijpers A. 2013. Evaluation of the sea
31 1027 ice proxy IP₂₅ against observational and diatom proxy data in the SW Labrador Sea.
32 1028 *Quaternary Science Reviews* **79**: 53-62.
- 33
34 1029 Werner K, Spielhagen RF, Bauch D, Hass HC, Kandiano E. 2013. Atlantic Water advection
35 1030 versus sea ice advances in the eastern Fram Strait during the last 9 ka: Multi proxy evidence
36 1031 for a two-phase Holocene. *Paleoceanography* **28**: 283-295.
- 37
38 1032 Werner K, Frank M, Teschner C, Müller J, Spielhagen RF. 2014. Neoglacial change in deep
39 1033 water exchange and increase of sea ice transport through eastern Fram Strait: evidence from
40 1034 radiogenic isotopes. *Quaternary Science Reviews* **92**: 190-207.
- 41
42 1035 Wilson LJ, Hald M, Godtliobsen F. 2011. Foraminiferal faunal evidence of twentieth-century
43 1036 Barents Sea warming. *The Holocene* **21(4)**: 527-537.
- 44
45 1037 Woodgate RA, Weingartner TJ, Lindsay R. 2010. The 2007 Bering Strait oceanic heat flux
46 1038 and anomalous Arctic sea-ice retreat. *Geophysical Research Letters* **37**: L01602.
- 47
48 1039 Xiao X, Fahl K, Stein R, 2013. Biomarker distributions in surface sediments from the Kara
49 1040 and Laptev seas (Arctic Ocean): indicators for organic-carbon sources and sea ice coverage.
50 1041 *Quaternary Science Reviews* **79**: 40-52.
- 51
52 1042 Xiao X, Fahl K, Müller J, Stein R. 2015a. Sea ice distribution in the modern Arctic Ocean:
53 1043 Biomarker records from trans-Arctic Ocean surface sediments. *Geochimica Cosmochimica*
54 1044 *Acta* **155**: 16-29.

- 1
2
3 1045 Xiao X, Stein R, Fahl K. 2015b. MIS 3 to MIS 1 temporal and LGM spatial variability in
4 1046 Arctic Ocean sea ice cover: Reconstruction from biomarkers. *Paleoceanography* **30**: 969-983.
5
6 1047 Yang S, Christensen JH. 2012. Arctic sea ice reduction and European cold winters in CMIP5
7 1048 climate change experiments. *Geophysical Research Letters* **39**: L20707.
8
9 1049 Zamelczyk K, Rasmussen TL, Husum K, Haflidason H, de Vernal A, Krogh Ravna E, Hald
10 1050 M, Hillaire-Marcel C. 2012. Paleooceanographic changes and calcium carbonate dissolution in
11 1051 the central Fram Strait during the last 20 ka yr. *Quaternary Research* **78**: 405-416
12
13 1052 Zamelczyk K, Rasmussen TL, Husum K, Hald M. 2013. Marine calcium carbonate
14 1053 preservation vs. climate change over the last two millennia in the Fram Strait: Implications for
15 1054 planktic foraminiferal paleostudies. *Marine Micropaleontology* **98**: 14-27.
16
17 1055 Årthun M, Eldevik T, Smedsrud LH, Skagseth Ø, Ingvaldsen R. 2012. Quantifying the
18 1056 influence of Atlantic heat on Barents Sea ice variability and retreat. *Journal of Climate* **25**:
19 1057 4736-4743.
20
21
22
23
24
25
26
27
28
29
30
31
32
33
34
35
36
37
38
39
40
41
42
43
44
45
46
47
48
49
50
51
52
53
54
55
56
57
58
59
60

1058 **Figure captions**

1059 Table 1. Depth-age model of NP05-11-70GC calibrated using Calib 6.1.1 (Stuiver and
 1060 Reimer, 1993), the Marine09 calibration curve (Reimer *et al.*, 2009) and a local reservoir age
 1061 (ΔR) of 105 ± 24 after Mangerud *et al.* (2006).

1062 Figure 1. The modern oceanography is presented on a bathymetric map of the Barents Sea
 1063 area. The core location of NP05-11-70GC is indicated by a black star, whereas previously
 1064 published records are indicated by number: (1) Risebrobakken *et al.* (2010), (2) Wilson *et al.*
 1065 (2011), (3) Berben *et al.* (2014), (4) Rasmussen *et al.* (2007), (5) Müller *et al.* (2012); Werner
 1066 *et al.* (2013), (6) Skirbekk *et al.* (2010); Jernas *et al.* (2013), (7) Müller *et al.* (2009), (8)
 1067 Slubowska *et al.* (2005); Jernas *et al.* (2013), (9) Klitgaard Kristensen *et al.* (2013), (10)
 1068 Lubinski *et al.* (2001), (11) Duplessy *et al.* (2001); (2005), (12) Risebrobakken *et al.* (2011),
 1069 and (13) Duplessy *et al.* (2005). Northern Barents Sea Opening (NBSO), Barents Sea
 1070 Opening (BSO), Barents Sea Exit (BSX). (a) The main surface currents (Hopkins, 1991).
 1071 Atlantic Water (red): Norwegian Atlantic Current (NwAC), North Cape Current (NCaC),
 1072 West Spitsbergen Current (WSC), Return Atlantic Current (RAC), Yermak Branch (YB) and
 1073 Svalbard Branch (SB). Polar Water (blue): Bear Island Current (BIC) and East Spitsbergen
 1074 Current (ESC). Coastal Water (black). (b) Seasonal sea ice margins (April (purple) and
 1075 August (orange)) for the period 1981–2010 (National Snow and Ice Data Centre (NSIDC)
 1076 Boulder Colorado, www.nsidc.com). The observed sea ice margin for April (dotted) and
 1077 August (dashed) from historical data for four sub-periods between 1870 and 2002: 1870–1920
 1078 (red), 1921–1961 (yellow), 1962–1988 (pink) and 1989–2002 (black) (Divine and Dick,
 1079 2006). (c) Temperature (black) and Salinity (grey) profile at the NP05-11-70GC core site
 1080 (78.40° N, 32.42° E). Water masses are defined according Gammelsrød *et al.* (2009).

1081 Figure 2. Depth-age model of NP05-11-70GC. Calibrated radiocarbon ages versus depth with
 1082 a linear interpolation between the dated levels. Error bars indicate the sampled depth intervals
 1083 and a $2\text{-}\sigma$ error on the calibrated ages.

1084 Figure 3. Biomarker analysis versus cal a BP and core depth. The black diamonds on the Y-
 1085 axis denote the AMS ^{14}C converted to calibrated radiocarbon ages. (a) Sea ice biomarker IP₂₅
 1086 versus age. (b) Phytoplankton biomarker brassicasterol versus age. (c) Phytoplankton-derived
 1087 HBI III biomarker versus age. Biomarker concentrations are normalized to total organic
 1088 carbon (black) and to sediment mass (grey). (d) Total organic carbon versus age. (e) P_BIP₂₅
 1089 versus age. (f) P_{III}IP₂₅ versus age. $>5\%$ summer sea ice concentration (SuSIC) is also
 1090 indicated when P_{III}IP₂₅ exceeds a value of 0.8 (Smik *et al.*, 2016). (g) Estimated spring sea ice
 1091 concentration (SpSIC) versus age.

1092 Figure 4. Planktic foraminiferal fauna and preservation indicator analysis versus cal a BP and
 1093 core depth. The black diamonds on the Y-axis denote the AMS ^{14}C converted to calibrated
 1094 radiocarbon ages. (a) Total planktic foraminiferal concentration versus age. (b) Planktic
 1095 foraminiferal fragmentation versus age. (c) Mean shell weight of *N. pachyderma* versus age.
 1096 (d-i) Species-specific relative abundance versus age.

1097 Figure 5. Stable isotopes analysis performed on *N. pachyderma* versus cal a BP and core
 1098 depth. The black diamonds on the X-axis denote the AMS ^{14}C converted to calibrated
 1099 radiocarbon ages. (a) $\delta^{18}\text{O}$ measurements corrected for ice volume effect after Fairbanks
 1100 (1989) (black) and uncorrected $\delta^{18}\text{O}$ measurements (grey) versus age. (b) $\delta^{13}\text{C}$ measurements
 1101 versus age.

1
2
3 1102 Figure 6. Multi-proxy analysis versus cal a BP and core depth. The black diamonds on the Y-
4 1103 axis denote the AMS ^{14}C converted to calibrated radiocarbon ages. (a) July insolation at 78°N
5 1104 (Laskar *et al.*, 2004) (note the reversed axis) versus age. (b) Sea ice biomarker IP_{25} versus
6 1105 age. Concentrations are normalized to total organic carbon (black line) and to sediment mass
7 1106 (grey line). (c) $\text{P}_{\text{III}}\text{IP}_{25}$ versus age. $>5\%$ summer sea ice concentration (SuSIC) is also
8 1107 indicated when $\text{P}_{\text{III}}\text{IP}_{25}$ exceeds a value of 0.8 (Smik *et al.*, 2016). (d) Estimated spring sea ice
9 1108 concentration (SpSIC) versus age. (e) $\delta^{18}\text{O}$ measurements corrected for ice volume effect after
10 1109 Fairbanks (1989) versus age. (f) Relative abundance of *N. pachyderma* versus age. (g)
11 1110 Planktic foraminiferal concentration versus age. (b-d) The in dark grey highlighted period
12 1111 reflects decreased sea ice conditions, whereas the in light grey highlighted periods indicate
13 1112 increased sea ice conditions. (e-g) The in grey highlighted periods are characterized by an
14 1113 increased influence of Atlantic Water.

15
16
17 1114 Figure 7. Illustrations of the proposed seasonal sea ice scenarios at the NP05-11-70GC core
18 1115 location (black star). The shaded areas surrounding the dotted lines represent the proposed
19 1116 variability of the sea ice margin for March (black), April (purple) and August (orange),
20 1117 whereas the numbers indicate the core locations of previous studies: (1) Berben *et al.* (2014),
21 1118 (2) Müller *et al.* (2012), (3) Müller *et al.* (2009), (4) Klitgaard Kristensen *et al.* (2013), and
22 1119 (5) Duplessy *et al.* (2001). (a) Period I. (b) Period II. (c) Period III (dotted lines with shaded
23 1120 areas) and present day situation (full lines) based on mean sea ice margins (1981–2010)
24 1121 (National Snow and Ice Data Centre (NSIDC) Boulder Colorado, www.nsidc.com).

25
26
27 1122
28
29
30
31
32
33
34
35
36
37
38
39
40
41
42
43
44
45
46
47
48
49
50
51
52
53
54
55
56
57
58
59
60

1123 Table 1

1124

Lab ID	Core depth (cm)	Material	Uncorrected AMS ¹⁴ C age	1σ	Calibrated age 2-σ range	Calibrated age used in depth-age model (cal a BP)
Beta-331327	37 - 43	Benthic foraminifera	2780	30	2281–2496	2389
Beta-346803	67 - 72	Benthic foraminifera	6110	40	6298–6536	6417
Beta-331328	122 - 127	Benthic foraminifera	8870	50	9307–9527	9417
Beta-331329	213 - 230	Benthic foraminifera	> 43500			

1125

"Disclaimer: This is a pre-publication version. Readers are recommended to consult the full published version for accuracy and citation."

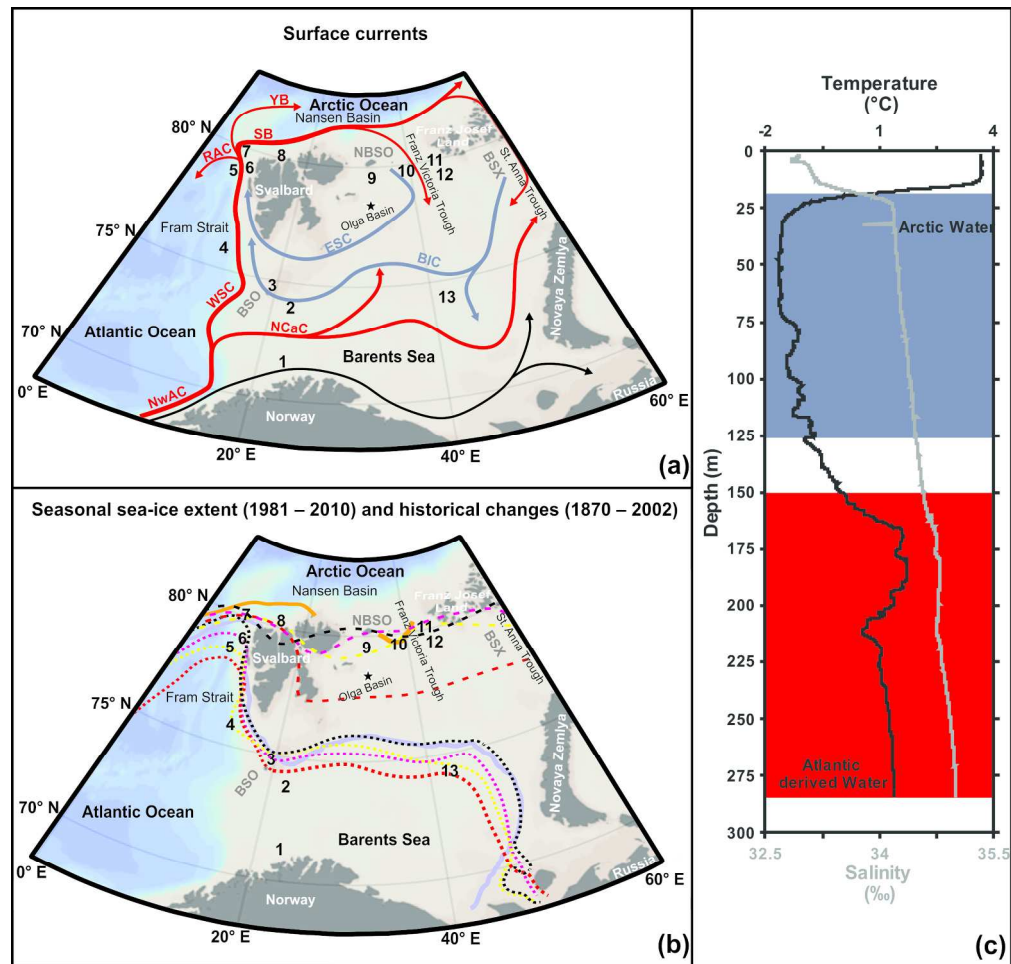


Figure 1. The modern oceanography is presented on a bathymetric map of the Barents Sea area. The core location of NP05-11-70GC is indicated by a black star, whereas previously published records are indicated by number: (1) Risebrobakken et al. (2010), (2) Wilson et al. (2011), (3) Berben et al. (2014), (4) Rasmussen et al. (2007), (5) Müller et al. (2012); Werner et al. (2013), (6) Skirbekk et al. (2010); Jernas et al. (2013), (7) Müller et al. (2009), (8) Slubowska et al. (2005); Jernas et al. (2013), (9) Klitgaard Kristensen et al. (2013), (10) Lubinski et al. (2001), (11) Duplessy et al. (2001); (2005), (12) Risebrobakken et al. (2011), and (13) Duplessy et al. (2005). Northern Barents Sea Opening (NBSO), Barents Sea Opening (BSO), Barents Sea Exit (BSX). (a) The main surface currents (Hopkins, 1991). Atlantic Water (red): Norwegian Atlantic Current (NwAC), North Cape Current (NCaC), West Spitsbergen Current (WSC), Return Atlantic Current (RAC), Yermak Branch (YB) and Svalbard Branch (SB). Polar Water (blue): Bear Island Current (BIC) and East Spitsbergen Current (ESC). Coastal Water (black). (b) Seasonal sea ice margins (April (purple) and August (orange)) for the period 1981–2010 (National Snow and Ice Data Centre (NSIDC) Boulder Colorado, www.nsidc.com). The observed sea ice margin for April (dotted) and August (dashed) from historical data for four sub-periods between 1870 and 2002: 1870–1920 (red), 1921–1961 (yellow), 1962–1988 (pink) and 1989–2002 (black) (Divine and Dick, 2006). (c) Temperature (black) and Salinity (grey) profile at the NP05-11-70GC core site (78.40° N, 32.42° E). Water masses are defined according Gammelsrød et al. (2009).

210x202mm (300 x 300 DPI)

" Disclaimer: This is a pre-publication version. Readers are recommended to consult the full published version for accuracy and citation."

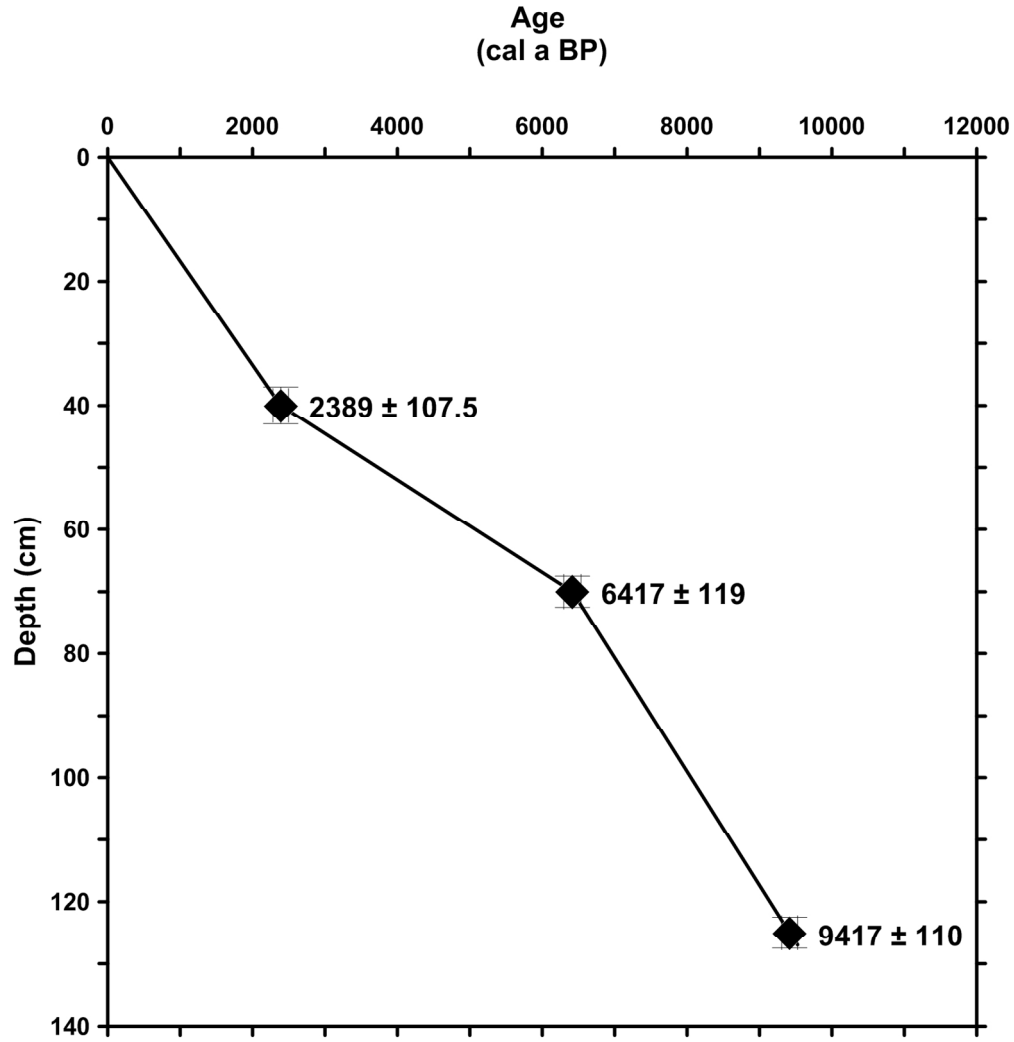


Figure 2. Depth-age model of NP05-11-70GC. Calibrated radiocarbon ages versus depth with a linear interpolation between the dated levels. Error bars indicate the sampled depth intervals and a 2-σ error on the calibrated ages.

146x151mm (300 x 300 DPI)

" Disclaimer: This is a pre-publication version. Readers are recommended to consult the full published version for accuracy and citation."

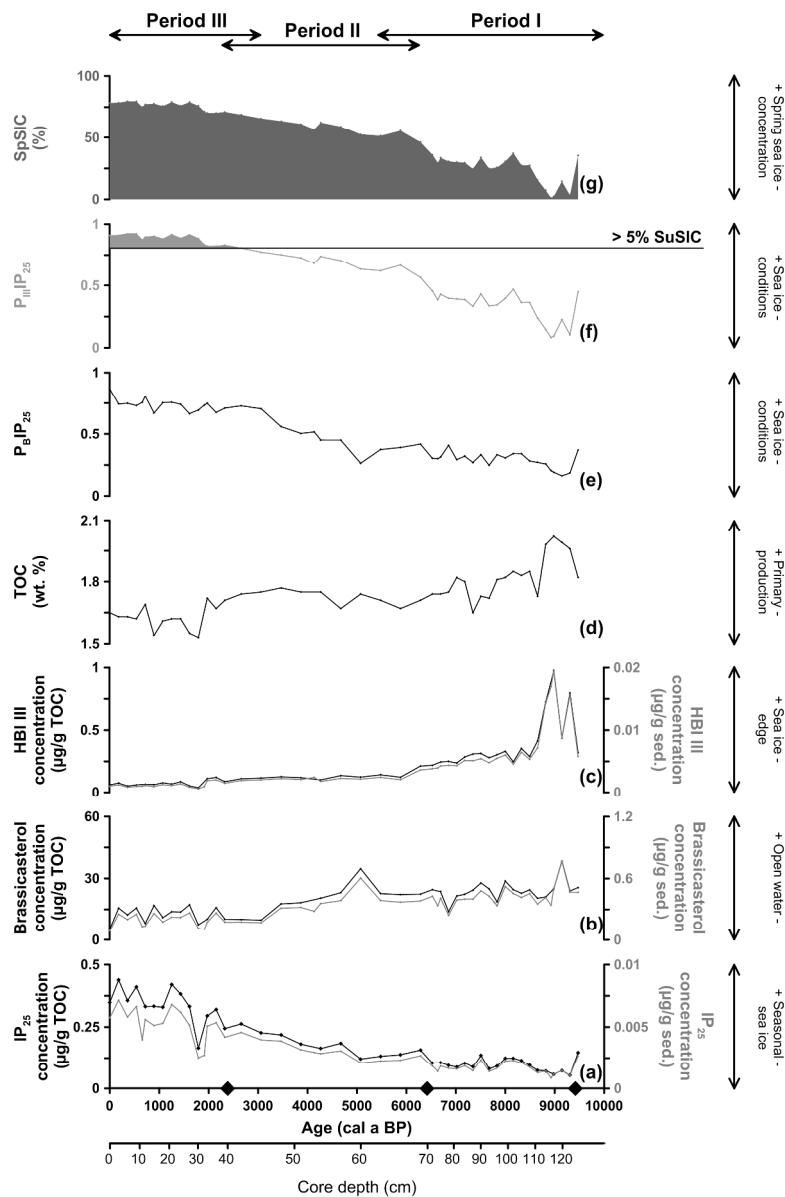


Figure 3. Biomarker analysis versus cal a BP and core depth. The black diamonds on the Y-axis denote the AMS 14C converted to calibrated radiocarbon ages. (a) Sea ice biomarker IP25 versus age. (b) Phytoplankton biomarker brassicasterol versus age. (c) Phytoplankton-derived HBI III biomarker versus age. Biomarker concentrations are normalized to total organic carbon (black) and to sediment mass (grey). (d) Total organic carbon versus age. (e) PBIP25 versus age. (f) PIIIIP25 versus age. >5% summer sea ice concentration (SuSIC) is also indicated when PIIIIP25 exceeds a value of 0.8 (Smik et al., 2016). (g) Estimated spring sea ice concentration (SpSIC) versus age.

199x308mm (300 x 300 DPI)

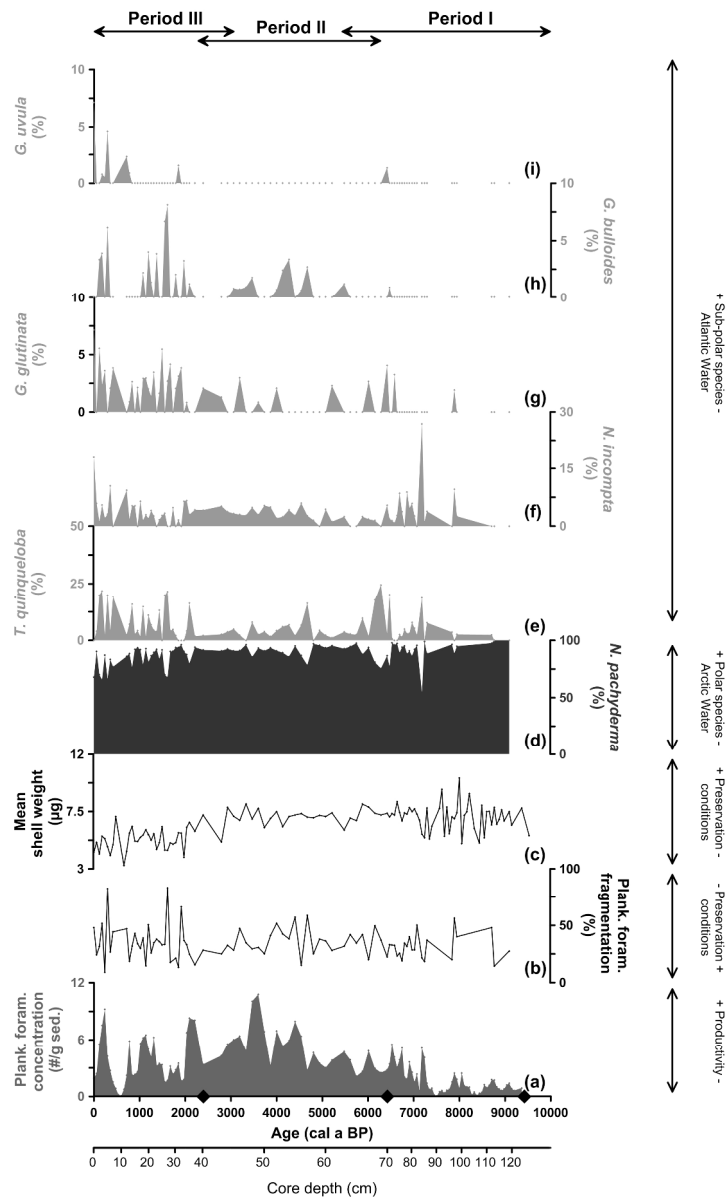


Figure 4. Planktic foraminiferal fauna and preservation indicator analysis versus cal a BP and core depth. The black diamonds on the Y-axis denote the AMS 14C converted to calibrated radiocarbon ages. (a) Total planktic foraminiferal concentration versus age. (b) Planktic foraminiferal fragmentation versus age. (c) Mean shell weight of *N. pachyderma* versus age. (d-i) Species-specific relative abundance versus age.

198x334mm (300 x 300 DPI)

"Disclaimer: This is a pre-publication version. Readers are recommended to consult the full published version for accuracy and citation."

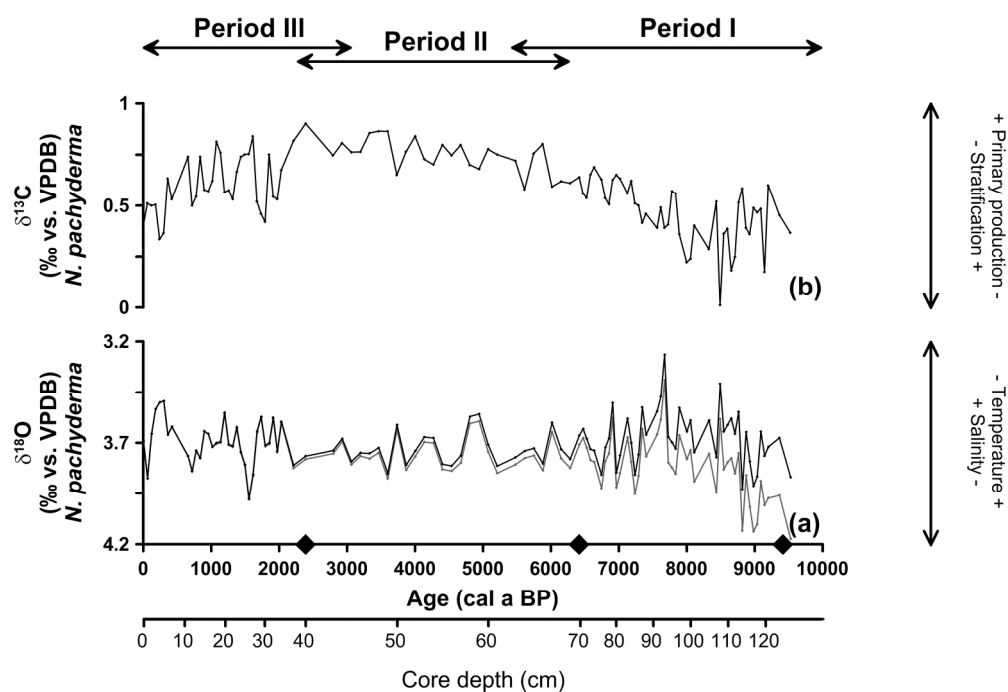


Figure 5. Stable isotopes analysis performed on *N. pachyderma* versus cal a BP and core depth. The black diamonds on the X-axis denote the AMS ^{14}C converted to calibrated radiocarbon ages. (a) $\delta^{18}\text{O}$ measurements corrected for ice volume effect after Fairbanks (1989) (black) and uncorrected $\delta^{18}\text{O}$ measurements (grey) versus age. (b) $\delta^{13}\text{C}$ measurements versus age.

187x130mm (300 x 300 DPI)

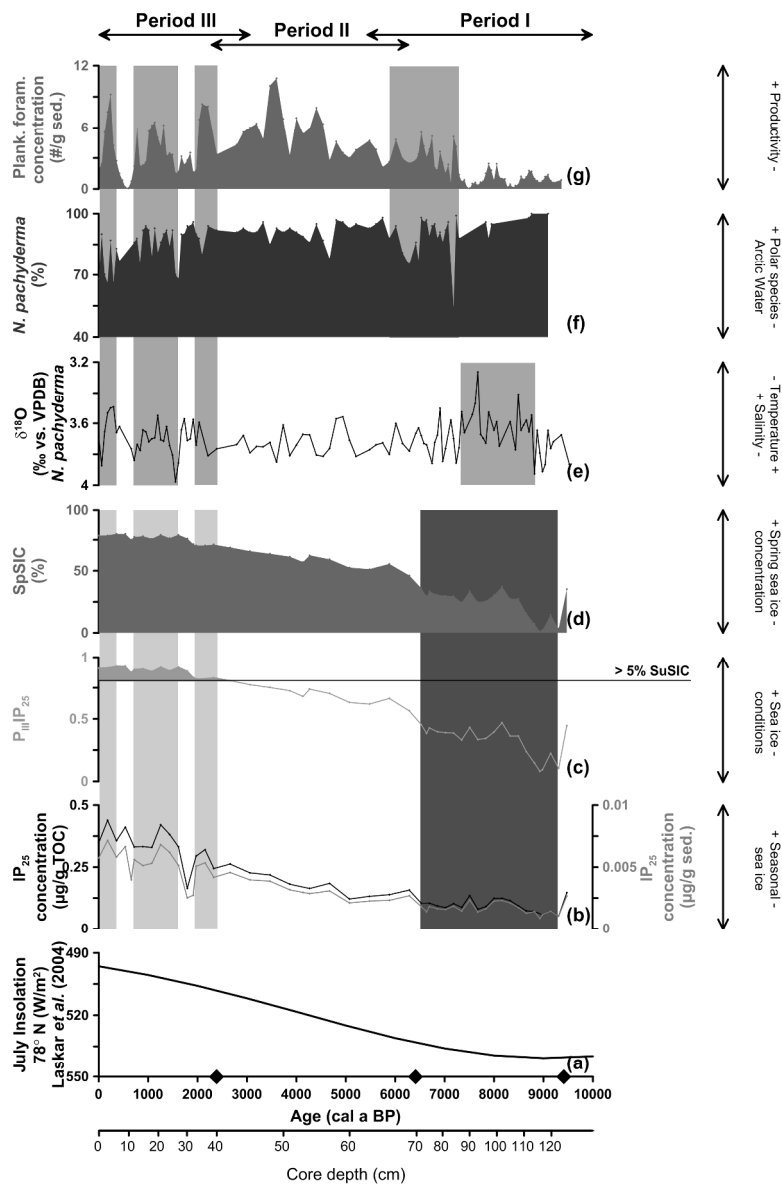


Figure 6. Multi-proxy analysis versus cal a BP and core depth. The black diamonds on the Y-axis denote the AMS 14C converted to calibrated radiocarbon ages. (a) July insolation at 78° N (Laskar et al., 2004) (note the reversed axis) versus age. (b) Sea ice biomarker IP25 versus age. Concentrations are normalized to total organic carbon (black line) and to sediment mass (grey line). (c) PIIIIP25 versus age. >5% summer sea ice concentration (SuSIC) is also indicated when PIIIIP25 exceeds a value of 0.8 (Smik et al., 2016). (d) Estimated spring sea ice concentration (SpSIC) versus age. (e) $\delta^{18}\text{O}$ measurements corrected for ice volume effect after Fairbanks (1989) versus age. (f) Relative abundance of *N. pachyderma* versus age. (g) Planktic foraminiferal concentration versus age. (b-d) The in dark grey highlighted period reflects decreased sea ice conditions, whereas the in light grey highlighted periods indicate increased sea ice conditions. (e-g) The in grey highlighted periods are characterized by an increased influence of Atlantic Water.

198x308mm (300 x 300 DPI)

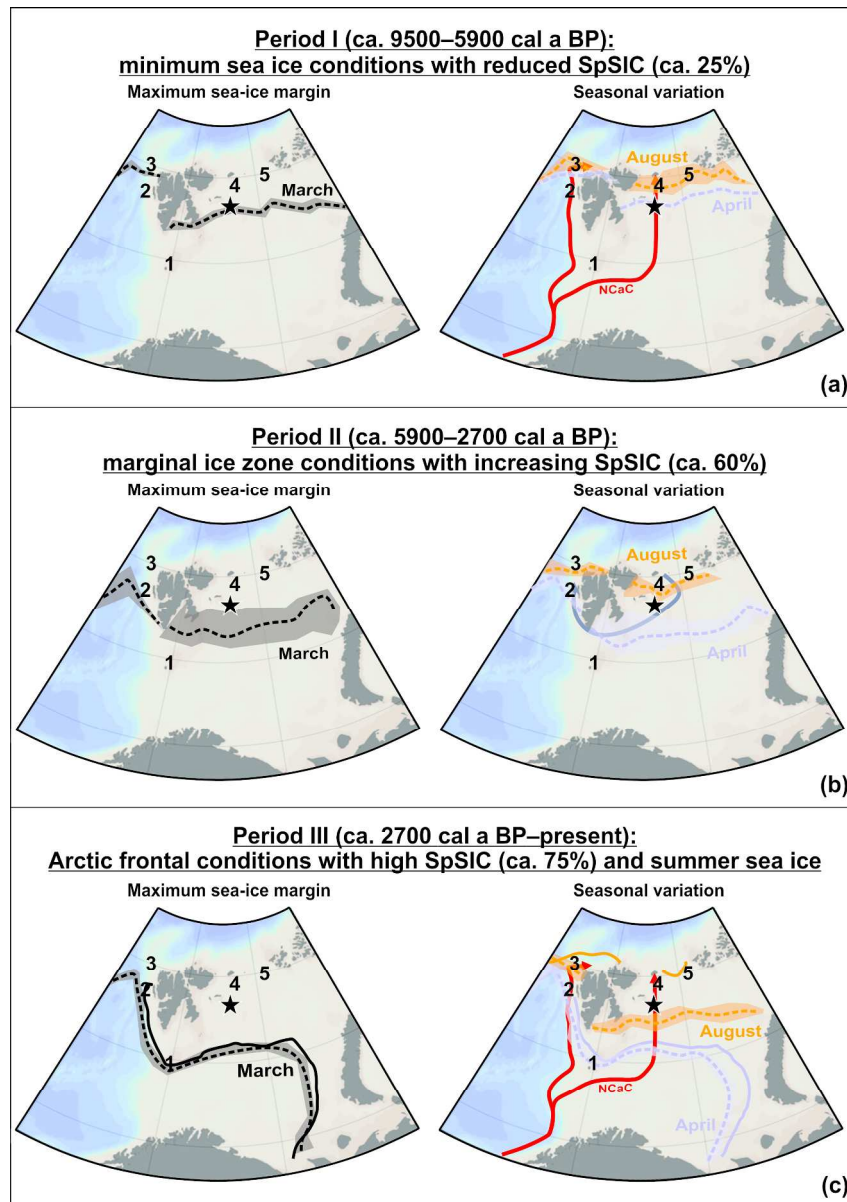


Figure 7. Illustrations of the proposed seasonal sea ice scenarios at the NP05-11-70GC core location (black star). The shaded areas surrounding the dotted lines represent the proposed variability of the sea ice margin for March (black), April (purple) and August (orange), whereas the numbers indicate the core locations of previous studies: (1) Berben et al. (2014), (2) Müller et al. (2012), (3) Müller et al. (2009), (4) Klitgaard Kristensen et al. (2013), and (5) Duplessy et al. (2001). (a) Period I. (b) Period II. (c) Period III (dotted lines with shaded areas) and present day situation (full lines) based on mean sea ice margins (1981–2010) (National Snow and Ice Data Centre (NSIDC) Boulder Colorado, www.nsidc.com).

210x296mm (300 x 300 DPI)